MJFAS
Malaysian Journal of Fundamental and Applied Sciences

Wahyuningsih *et al.* | Malaysian Journal of Fundamental and Applied Sciences, Vol. 22 (2026) 166–186

RESEARCH ARTICLE

# From Traditional Food to Nutraceuticals: LC-HRMS Identifies Leaves and Roots Antidiabetic Metabolites of *Amaranthus spinosus* L. and *Amaranthus viridis* L. from Buru Island (Wallacea Areas)

**Sri Wahyuningsih, Bambang Retnoaji, Rarastoeti Pratiwi, L. Hartanto Nugroho***

Faculty of Biology, Gadjah Mada University, Yogyakarta 55281, Indonesia

Abstract The leaves and roots of *A. spinosus* and *A. viridis* on Buru Island (Wallacea region) as antidiabetics have received little attention. The goal of this study was to identify active chemicals in the leaves and roots of these two plant species that could be used as antidiabetic nutraceuticals. The method in this research used five approaches: LC-HRMS, chemometric analysis, volcano plot, Venn diagram, and in silico. The results showed that the roots of both plant species had the highest chemical diversity, especially in the acid, lipid, and derivative groups. The specific compounds identified consisted of LAS (8), LAV, RAS (13), and RAV (14). In silico analysis indicated 25-Dihydroxyvitamin D3 and ursolic acid from the RAS sample as two of the best potential antidiabetic alternatives, with binding energies of (-10.1 kcal/mol) and (-9.7 kcal/mol) to the COX-2 protein, respectively. On the other hand, the positive control (diclofenac) showed a weaker binding energy of -7.5 kcal/mol. In conclusion, 25-Dihydroxyvitamin D3 and ursolic acid compounds have a strong inhibitory effect on COX-2 protein, indicating that they are viable natural candidates for the development of future antidiabetic therapies.

Keywords: *Amaranthus*, antidiabetic, *in-silico*, LC-HRMS, metabolomic, nutraceutical.

## Introduction

The historical consumption of *Amaranthus* species as a vegetable food and medicine is attributed to their abundance of nutrients and bioactive compounds, including flavonoids and betalains, known for their antioxidant and antidiabetic effects [1, 2]. *A. spinosus* and *A. viridis*, two *Amaranthus* species with a broad tropical and subtropical distribution, have a history of traditional uses attributed to their therapeutic properties. In vitro and in vivo tests confirm the leaf extracts and mixed organs from both species have potential antihyperglycemic efficacy [3]. However, both species remain understudied for some reason, with limited phytochemical data available.

Phytochemical can study with metabolomic approach. This approach is a complete analysis chemical characterization, for discovering compound variety, and for increasing the use of the biological activity compounds in various food crops and medicinal species [3]. A previous study on *Amaranthus* species (*A. hybridus, A. blitum, and A. caudatus*) uses LC-MS/MS and $^{1}$H-NMR found significant metabolic diversity in both wild and cultivated plants [3, 4]. This outcome is influenced by environmental conditions, production methods, organs, and plant age. Araujo-León *et al*. (2024) investigates the metabolomic profiles of A. cruentus leaves and flowers using HPLC and identified variation in the metabolomic profiles and distribution of flavonoids, cinnamic acid derivatives, and betalains between the two organs [5].

Currently, most metabolomic research on Amaranthus is limited to a specific group of species (e.g., *A. cruentus, A. hybridus, A. tricolor, A. retroflexus*) that focuses on the upper parts of the plant, namely edible leaves or flowers, with little attention paid to the roots or the distribution of antidiabetic metabolites in various organs [3, 5]. In fact, the combination of Amaranthus species roots and other medicinal plants

***For correspondence:**
hartantonugroho2005@ugm.ac.id

**Received:** 18 Nov. 2025
**Accepted:** 7 Jan. 2026

in vivo is antioxidant and hypoglycemic. These results indicate that there are various bioactive compounds associated with glucose, lipid, and oxidative stress regulation in hidden organs [6]. This discovery opens up a knowledge gap, notably in the comparative metabolomics in leaves and root organs both above and below the surface. Furthermore, systematic mapping of antidiabetic metabolites bases on LC-HRMS in the leaves and roots of *A. spinosus* and *A. viridis*, as well as explicit comparison of their metabolic signatures, is still unavailable. This gap limits the rational selection of plant parts for nutraceutical development and standardization.

An additional gap that has not received much attention is geographical uniqueness. Indonesia has three main phytogeographical regions: the Sunda Shelf, the Sahul Shelf, and Wallacea, which support its biodiversity. Buru Island (Maluku) is part of Wallacea and has high plant endemism and ecological divergence compared to the surrounding continental shelf due to its complex geological history, seasonal monsoon climate, and strong isolation in the form of a sea barrier [7]. The species list for Indonesia and the Maluku Islands emphasizes that Wallacea harbors unique lineages and locally distinct assemblages of plants, characterized by adaptive traits specific to extreme environments. These environmental filters and evolution are thought to shape the repertoire of secondary metabolites, yet metabolomic studies explicitly related to Wallacean origins are still almost nonexistent [8].

This regional disparity must be acknowledged in the context of nutraceutical research. Metabolomic studies across many genera have shown that metabolic variations influenced by environmental and origin factors can facilitate the discovery of novel diabetic treatments. The Wallacea flora is distinctive due to its exposure to a temperature regime that differs from that of the Sunda and Sahul areas [7, 8]. Consequently, *A. spinosus* and *A. viridis*, representing worldwide populations of the species on Buru Island, may include a distinctive array of metabolites, potentially containing undiscovered antidiabetic chemicals or atypical combinations of established compound groups.

Nutraceuticals represent a modern advancement that integrates conventional knowledge with precise analytical techniques, particularly Liquid Chromatography-High Resolution Mass Spectrometry (LC-HRMS) [9, 10]. Unlike conventional phytochemical screening, LC-HRMS allows simultaneous detection and structural elucidation of hundreds of compounds down to picomolar concentrations with mass accuracy <5 ppm [10, 11]. This method has successfully identified 14 antidiabetic compounds in *Artemisia annua*, including sesquiterpene lactone derivatives that were not detected by traditional techniques [12].

As a result, The present study addresses these knowledge gaps by applying LC-HRMS–based metabolomics to identify and compare antidiabetic metabolites in leaves and roots of *Amaranthus* spinosus L. and *Amaranthus* viridis L. collected from Buru Island, a representative Wallacea locality [7, 8]. By integrating organ-specific metabolite profiling with prior pharmacological evidence on enzyme inhibition and glucose-lowering actions of these species [3, 6], this work seeks to (i) map the distribution of candidate antidiabetic metabolites between leaves and roots, (ii) highlight chemotaxonomic and biogeographical features that distinguish Wallacean *Amaranthus* material from previously studied populations, and (iii) propose promising plant parts and metabolite classes for development into standardized nutraceuticals targeting diabetic. Therefore, the study provides one of the first metabolomics-anchored contributions to valorizing Wallacea's plant diversity in the context of metabolic disease prevention and functional food innovation.

# Materials and Methods

## Chemicals

The Merck MeOH (Darmstadt, Germany) was used for sample extraction. MeOH (HPLC-grade), formic acid (0.1%), acetonitrile (ACN), water ($H_2O$), and nylon membrane filtration (0.2 µm) were produced by Fisher Scientific Korea Ltd. (Seoul, South Korea) and the United States for dilution and the mobile phase. The mobile phases consisted of solvent A (MS-grade water containing 0.1% formic acid) and solvent B (MS-grade acetonitrile containing 0.1% formic acid) for LC-HRMS analysis.

## Sample Preparation and Extraction

Plant samples of *A. spinosus* and *A. viridis* were collected from open fields in the Lolong Guba sub-district, Buru District, Maluku Province, Indonesia, in November 2024 (Figure 1). The plant materials were authenticated by Prof. Dr. Purnomo, M.S., at Gadjah Mada University and deposited in the Laboratory of Plant Systematics (Gadjah Mada University), Yogyakarta, Indonesia (Table 1). The ground leaves and roots (100 g) were dissolved with 99.8% MeOH (1 L) above room temperature for 48 hours,

evaporated with a rotary evaporator (RE-300; Stuart, UK) to produce a crude extract, and stored at 4°C. Additionally, the sample (10 mg) was mixed with MeOH (1000 µL, HPLC-grade) in a vortex over 1 minute and filtered with a nylon pore (0.2 µm) for LC-RHMS analysis [13, 14].

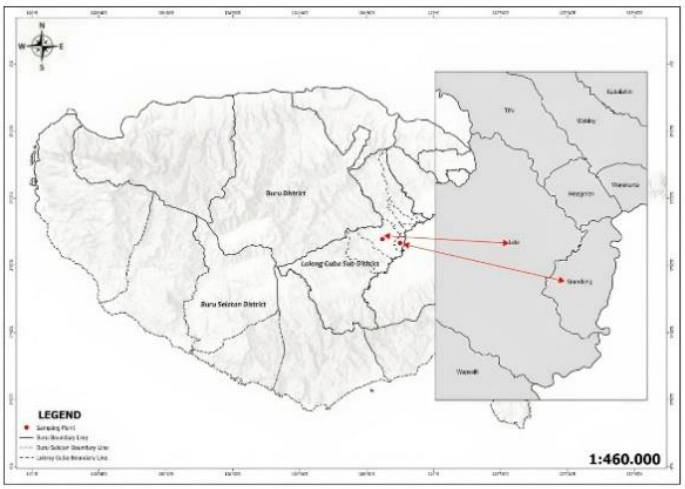


**Figure 1.** The study area map of Lolong Guba Sub-district, Buru Regency, Maluku Province, Indonesia, illustrates the sampling locations of *A. spinosus* and *A. viridis*. The elevation profile, indicated by the gradient legend, shows the topographic variation across the region

**Table 1.** *Amaranthus* species employed in this investigation

| No | Species | Registration and voucher number | Origin | Genus | Habitat |
|---|---|---|---|---|---|
| 1. | *A. spinosus* L. | 00741/S.bt/x/2024 | Vietnam & part of Africa | *Amaranthus* | Wild |
| 2. | *A. viridis* L. | 00740/S.bt/x/2024 | America | *Amaranthus* | Wild |

## LC-HRMS Analysis

Thermo Scientific™ Vanquish™ Horizon Ultra-High Performance Liquid Chromatography (UHPLC) (Germering, Germany) and Thermo Scientific™ Orbitrap™ Exploris 240 High Resolution Mass Spectrometry (HRMS) (Bremen, Germany) were connected to an Optamax™ NG Heated Electrospray Ionization (H-ESI) with a DuoSpray ion source (negative and positive modes). Separation was accomplished on the Thermo Scientific™ Accucore™ (Lithuania) Phenyl Hexyl column (100 mm x 2.1 mm x 2.6 µm) using a gradient mobile phase A: MS grade water with 0.1% formic acid and B: MS grade acetonitrile with 0.1% formic acid. Elution began at 5% B and steadily expanded to 90% in 16 minutes, remained at 90% for 4 minutes, and then returned to 5% B for 25 minutes. The column temperature was kept at 40°C, and the flow rate was set to 0.3 mL/minute. The injection volume was 5 µL.

The MS platform was run in information-dependent acquisition (IDA) mode, with full MS/dd-MS2 (polarity switching), resolution of 60,000 FWHM, mass range of 70-800 m/z, data-dependent fragmentation (dd-MS2) of 22,500 FWHM, and normalized collision energies of 30, 50, and 70 (nitrogen). The electrospray ionization (ESI) was executed at 320°C, utilizing an ion migration tunnel at 300°C and an ion spray voltage of 3500 V (positive mode) and 2500 V (negative mode). The sheath gas, auxiliary gas, and sweep gas were all set to 35 arbitrary units, 7 AU, and 1 AU, respectively.

## Data Mining and Statistical Examination

LC-HRMS data was processed using Thermo Scientific Compound Discoverer 3.3 software (San Jose, USA), which included mzCloud Library, Chemspider Database, and Mass List Search, in accordance with standard protocols for peak selection, chromatogram deconvolution, isotope peak grouping, and alignment. Features were identified at a density threshold of ±5 ppm and grouped by retention duration (0.2 minutes) [14]. The LC-HRMS data emerged by principal component analysis (PCA) and partial least squares discriminant analysis (PLS-DA), with sum normalization and autoscaling [15]. VIP scores ≥ 1 were implemented to determine distinct metabolites, as were volcano plots (FC > 1.5 and p-value < 0.05). The Venn diagram tool, found at https://bioinformatics.psb.ugent.be/webtools/Venn/software

(UGent Bioinformatics & Evolutionary Genomics), was used to identify and continue to investigate these unique metabolites [14, 15].

## *In-silico* Prediction

### Biological Activity Prediction as Antidiabetic

The canonical SMILES of distinct compounds from the samples were acquired via PubChem (https://pubchem.ncbi.nlm.nih.gov/) and inserted in the PASSonline web server (http://way2drug.com/passonline/predict.php). [16, 17]. The biological activity potential as an antidiabetic emerged by the Pa (active) [18]. Pa>Pi is recognized as probable for a specific chemical. Substances with Pa > 0.7 exhibit strong empirical activity. Those with Pa values of 0.5–0.7 offer modest activity but are distinct from existing medicines. In contrast, Pa < 0.5 indicates lower experimental activity but a greater probability of identifying New Chemical Entities (NCEs).

### Toxicity Analysis Prediction

The ProTox-3.0 online tool (https://tox.charite.de/protox3/) was utilized to measure the oral toxicity (mg/kg) values and toxicity classifications for each candidate. The platform is separated into five distinct classification processes: (1) acute toxicity (6 models); (2) organ toxicity (5 models); (3) toxicological endpoints (8 models); (4) toxicological pathways (12 models); and (5) toxicity targets (15 models) [19].

### Swiss ADME Evaluation

SwissADME is a tool that is used to estimate the ADME, pharmacokinetics, and drug-likeness properties of small molecules based on Lipinski's Rule of Five on the website (http://www.swissadme.ch). The comprehensive approach, from uploading the compound to evaluating the outcome, starts with the user downloading a small molecular structure in SMILES, SDF, or MOL format, or drawing with the integrated modeler. Furthermore, the user uploads, clicks the run button, and the website will calculate the parameter value [17, 18].

### Molecular docking

Ligand preparation: a total of compounds following RO5 from *A. spinosus* and *A. viridis* were used. The chemical structure of each compound was retrieved from the PubChem database and saved as an SDF format, which was then converted into PDB file format using BIOVIA Discovery Studio 2019.

Protein preparation: The three-dimensional (3D) structure of the target protein associated with the COX-2 diabetic protein was downloaded from the Protein Data Bank (PDB) database under PDB ID 1PXX and stored in PDB file format. This protein was in a complex with diclofenac. Additionally, water, natural ligands, and unnecessary components were removed from the protein structure [16].

Molecular docking simulation: Protein-ligand docking was performed using AutoDock Vina software integrated with PyRx 0.8. The docking output with a lower binding affinity score than the inhibitor indicates high potential as an antidiabetic [17, 19]. BIOVIA Discovery Studio 2019 is used for illustrating docking results, including the protein's ligand-binding location.

## Results and Discussion

### Morphological Features of Plant Materials

Morphological features in plants are not just for description. They determine how plants survive and reproduce in different environments, underpin species identification and breeding, and strongly influence community and ecosystem processes over both present and past climates [20]. Figure 2 showed the differences in morphology between *A. spinosus* and *A. viridis*, including leaf color, root structure and color, and overall plant morphology. *A. spinosus* exhibited darker green leaves with a slightly glossy texture, while *A. viridis* displayed lighter green. That pigmentation is influenced by genetic (chlorophyll content) and environmental factors. The root of *A. spinosus* has a less dense but deeper taproot system with white and red coloration for adaptability, competitive development in dense environments, attraction of particular symbiotic microorganisms, and defense against heavy metals, fungus, and bacteria [20-22]. In contrast, *A. viridis* displayed a more fibrous and extensive root network with a pale white color correlated with environmental conditions, root structure, cell turgor rate, chlorophyll composition, or accumulation of compounds such as suberin, lignin, or phenolics for a chemical barrier against soil-borne fungi, reduced microbial attraction (many pathogens target pigmented tissues), reduced water loss, nutrient, and stress resilience [23-26].

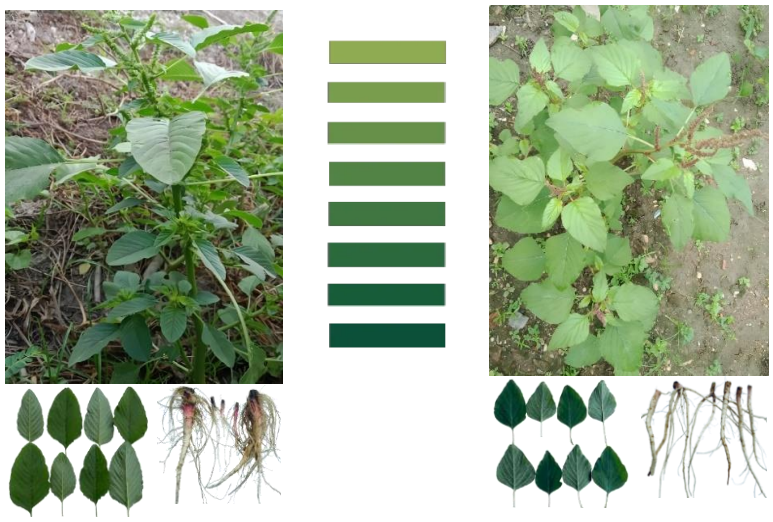

A B

**Figure 2.** Morphological features of (A) *A. spinosus* and *A. viridis* (B) found in Lolong Guba sub-district, Buru Regency, Indonesia. Each panel displays an entire plant (top); leaves and roots (bottom) to illustrate the diversity in colour

## LC–HRMS Metabolomic Profiling Analysis

The selection of analytical methods, particularly in metabolomic profiling, is a crucial step in research because it will affect the number of compounds detected. LC-HRMS is used because it is considered superior in mapping thousands of metabolites, proteins, and lipids and authenticating halal and haram foods comprehensively, both targeted and untargeted, which cannot be mapped by other instruments [12, 27]. In this study, based on the results of LC-HRMS analysis, ten groups of compounds were obtained, dominated by acids, lipids, and their derivatives in RAS and RAV samples (figure 3). The high levels of these two groups of compounds are due to organ function (physiology) and environmental adaptation [27-29].

The root systems are used to store and protect organs in the soil; consequently, they are additionally abundant in primary metabolites (e.g., organic acids, lipids, and their derivatives) associated with ion absorption, osmotic regulation, membrane structure, and signaling. Investigations of root exudates reveal the varied secretion of organic acids with significant internal concentrations. Moreover, roots have a higher concentration of organic acids and lipids than aerial portions, particularly under biotic and abiotic stress, as these substances serve as osmolytes, energy reserves, and structural elements for membranes and protective barriers [27-32].

Furthermore, the reason for the increased concentration of these two groups of compounds is that the samples grew in the Wallacea region (including Buru Island). The unique environmental conditions (tropical climate, distinct dry and wet seasons, and soil deficient in nutrients) increase the production of primary and secondary metabolites as an adaptive response in osmotic adjustment and protection against oxidative stress. Environmental metabolomics research shows that soil factors significantly shape root metabolite profiles, more than aerial parts, because roots directly detect soil pH, salinity, heavy metals, and nutrient status. In *A. viridis*, exposure to metal stress (Pb) increases citric acid and other organic acids and alters lipid peroxidation status in roots. [27, 33-36].

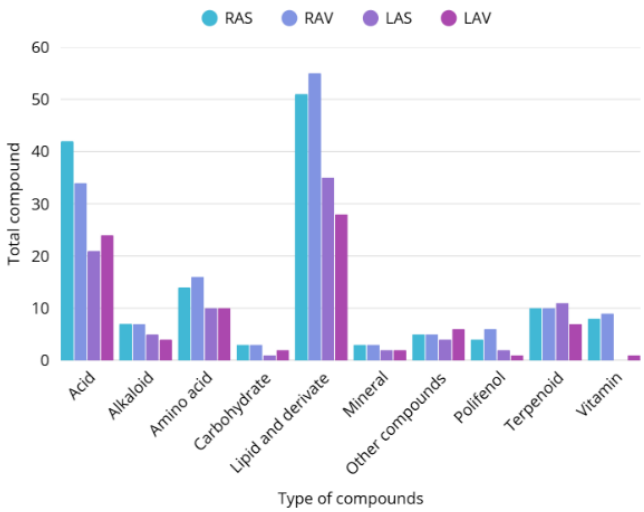


**Figure 3.** The accumulated concentration of phytochemical substances detected in (A) *A. spinosus* (LAS and RAS) and (B) *A. viridis* (LAV and RAV) metanol extracts utilizing LC-HRMS with negative (-) and positive (+) ionization

## Revealing Distinct Metabolites Between *A. spinosus* and *A. viridis*

The compounds obtained from the LC-HRMS chromatograms of leaf and root extracts were processed using chemometric analysis (PCA and PLS-DA), followed by volcano plot and Venn diagram analysis to reinforce and visualize the different compounds produced by each sample. Chemometric analysis aims to identify and classify different thousands of metabolites in a single two-dimensional graph [37, 38]. In contradistinction to PCA, which only explores the total variance of the data without considering group labels, PLS-DA is designed to distinguish groups by maximizing the variance between classes [39, 40].

Figure 4 and Figure 5 showed the score plots of PCA and PLS-DA in the sample organ. Overall, PC1 and PC2 values demonstrated over fifty percent of the variations, indicating the separation of compounds in each organ was attractive. These results are consistent with previous studies, which found that the cumulative variance explained by PC1 and PC2 in *Amaranthus* species is approximately 50% [41, 42]. PLS-DA is a discriminant analysis commonly used in metabolomic data analysis to classify data through data dimension reduction and combine regression models to obtain regression results based on specific discriminant thresholds. This model uses cross-validation with $R^2$ and $Q^2$ parameters. R2 explains the interpretability level of the model variables, and Q2 explains the predictability level of the model. Theoretically, good model results are obtained when the values of $R^2$ and $Q^2$ are closer to 1 and vice versa. Under normal conditions, the values of R2 and Q2 are greater than 0.05, and the disparity between the two should not be excessive. When the R2 value is low, the test set becomes unstable, whereas a low Q2 value suggests significant background noise in the test set or the existence of more aberrant items (outliers) in the model [42]. Cross validation of Q2 and R2 is used to select the number of components with the ideal range. $R2 > 0.7$ is considered substantial predictive ability, and Q2 should be close to R2, indicating that the data is fitting the model [43].

The cross validation in the PLS-DA for this study showed $R^2 = 0.99$, $Q^2 = 0.81$ in leaves (LAS, LAV), $R^2 = 0.99$, $Q^2 = 0.92$ in roots, and a p-value in two sample organs from the permutation test ($p > 0.05$) (Figure 5a and Figure 5b). The high $R^2$ and $Q^2$ values suggest a significant internal consistency within the examined groups [43]. Furthermore, the insignificant p-value from the permutation test ($p > 0.05$) represents a potential risk of overfitting because of the high-dimensional structure of the data. Thus, this model is regarded as an exploratory instrument for discovering prospective biomarkers rather than a conclusive prediction classifier [43].

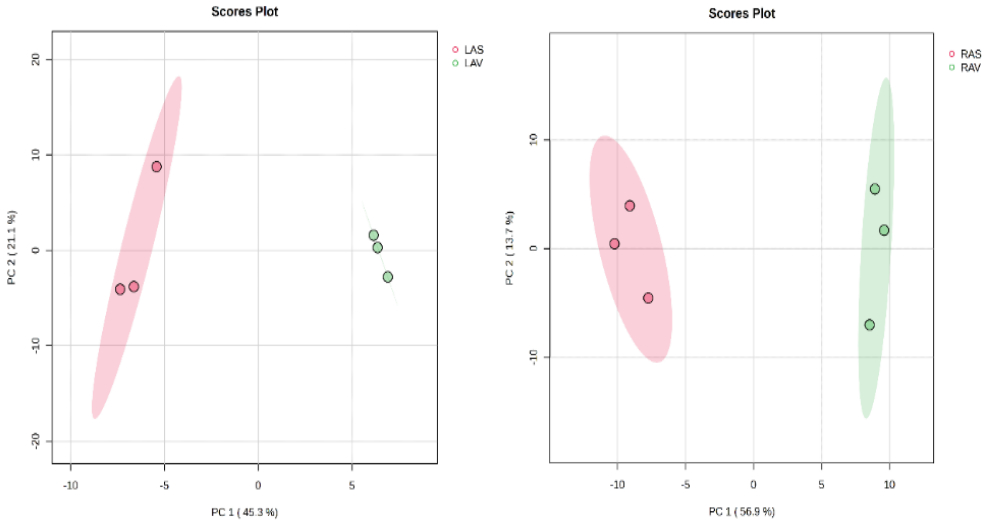


A B

**Figure 4.** Principal Component Analysis (PCA) score plots between *A. spinosus* and *A. viridis* Buru Island using MetaboAnalyst 6.0. (A) leaves (LAS and LAV); (A) roots (RAS and RAV) samples

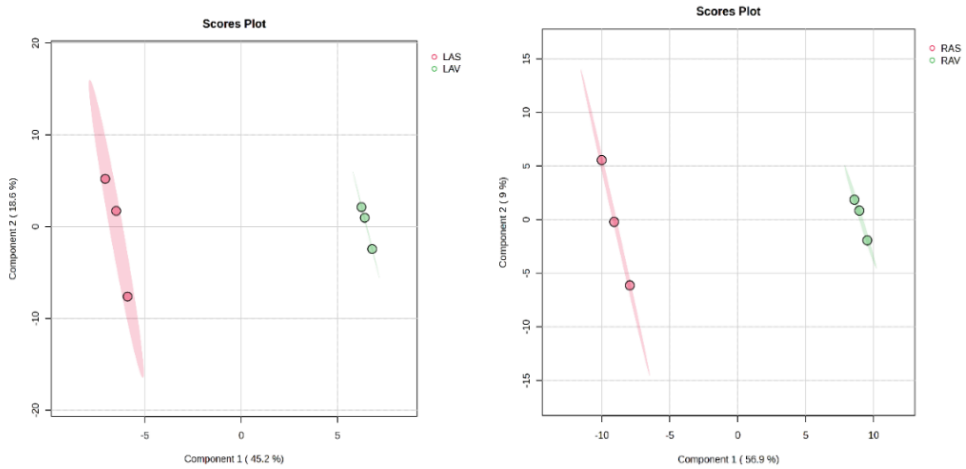


A B

**Figure 5.** Partial Least Squares-Discriminant Analysis (PLS-DA) score plots between *A. spinosus* and *A. viridis* Buru Island using MetaboAnalyst 6.0. (A) leaves (LAS, LAV); (B) roots (RAS, RAV) samples

The top 15 metabolites (>1.0 scores) in VIP summarized the most influential metabolites responsible for organ type discrimination and were selected for future investigation [40, 43, 44-46]. Among the top 15 discriminatory metabolites in leaves (LAS, LAV), pimelic acid, decanedioic acid, and oxohexenoic acid were identified as major contributors. In contrast, hexanoic acid, phosphatidic acid, and ursolic acid were identified as important for distinguishing root (RAS, RAV) organs (Figure 6b). A large number of these compounds have an extensive number of beneficial impacts, involving responses to inflammation, antioxidants [46–49], insulin sensitization, potential neurogenic effects, antiproliferative, antitumor, anti-angiogenesis, antidiabetic, anti-obesity, anticancer, and metabolic-regulating effects, apoptosis cell, and anti-Krabbe disease (globoid cell leukodystrophy) [50–52].

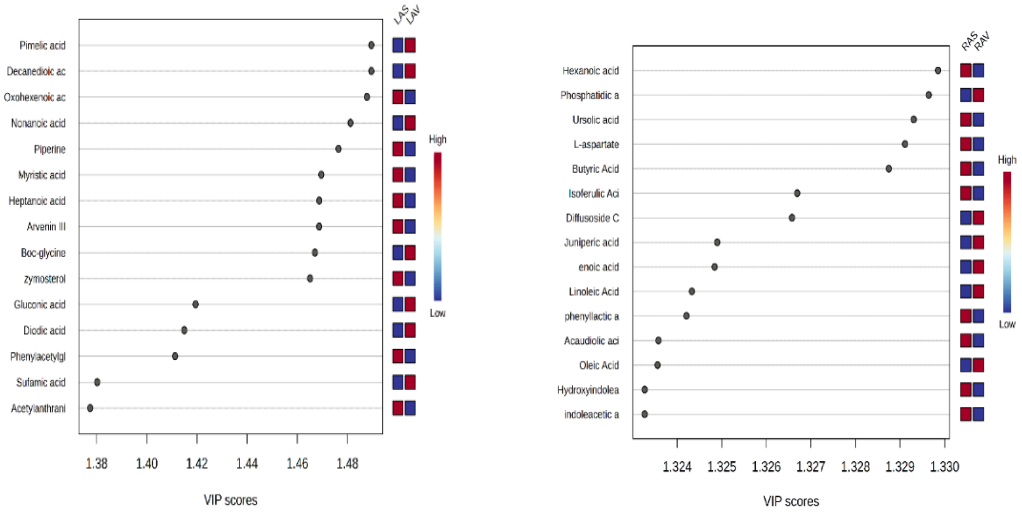


A B

**Figure 6.** Variable Importance in Projection (VIP) PLS-DA statistics between *A. spinosus* and *A. viridis* Buru Island using MetaboAnalyst 6.0 tools with Red signifies substantial concentrations and dark blue identifies impaired quantities. (A) leaves (LAS, LAV); (B) roots (RAS, RAV) samples

Figure 7 showed the volcano plot analysis. This analysis illustrates the statistical test results of thousands of variables simultaneously, facilitating the identification of the most biologically significant changes. In this study, the volcano plot was used to reinforce the identification of key metabolites based on VIP scores. The position of the points and color variations indicated the level of change in expressed abundance. The X-axis (Log2 FC) >1.5 indicates the extent of variation among groups, and the Y-axis (-log10 p-value) denotes the degree of statistically significant difference. The higher the position of a point on the Y-axis (origin 0.0), the lesser the p-value, which means the more significant the difference [53, 54].

Figure 7a showed that oxohexenoic acid, piperine, and arvenin III increased in the LAS sample and decreased in the LAV sample. Conversely, pimelic acid, decanedioic acid, and nonanoic acid increased in the LAV sample. Figure 7b shows that the compounds that increased in the RAS sample were hexanoic acid, ursolic acid, and L-aspartate, while in the RAV sample, they were phosphatidic acid, diffusoside C, and juniperic acid. These results show that each sample group has a unique chemical of what is happening inside the cells or tissues. The results in Figures 7a and 7b demonstrated that the statistical model effectively distinguished between the sample groups (LAS vs. LAV and RAS vs. RAV) according to their chemical compositions [53, 54].

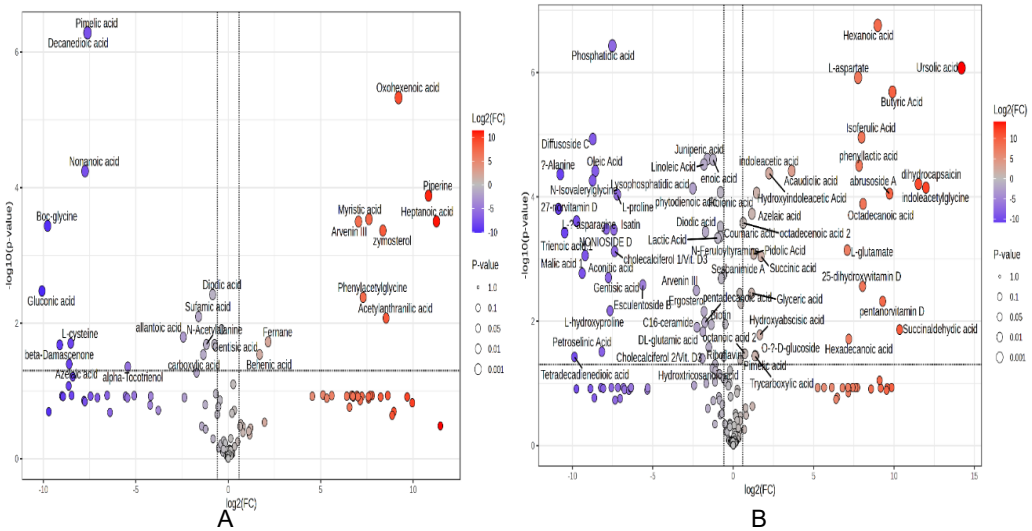


A B

**Figure 7.** Volcano plot illustrating the most discriminative metabolites. Blue dots indicate a significant decrease, red an increase, and grey no significant. (A) leaves (LAS vs LAV); (B) roots (RAS vs RAV) samples

Figure 8 shows a Venn diagram analysis that aims to visualize the comparison of metabolite composition among various sample groups. Unlike the volcano plot, which performs quality screening (vertical), the Venn diagram performs specificity screening (horizontal). However, both are instruments that work sequentially to filter the most valid biomarkers. Figure 8a displayed Venn diagram analysis for 48 different chemicals in leaves (LAS = 8, LAV = 13) and roots (RAS = 13, RAV = 14) in both *Amaranthus* species, indicating organ-specific metabolic pathways across aerial and subterranean tissues [56, 57]. Moreover, comparisons between species have similar compounds with 76 unique metabolites (Figure 8b). Furthermore, the detailed compounds can be shown in Table 2. This distinction confirmed that the differences in organs, genetics, and ecology factors have an impact on biosynthetic adaptations [58, 62, 63].

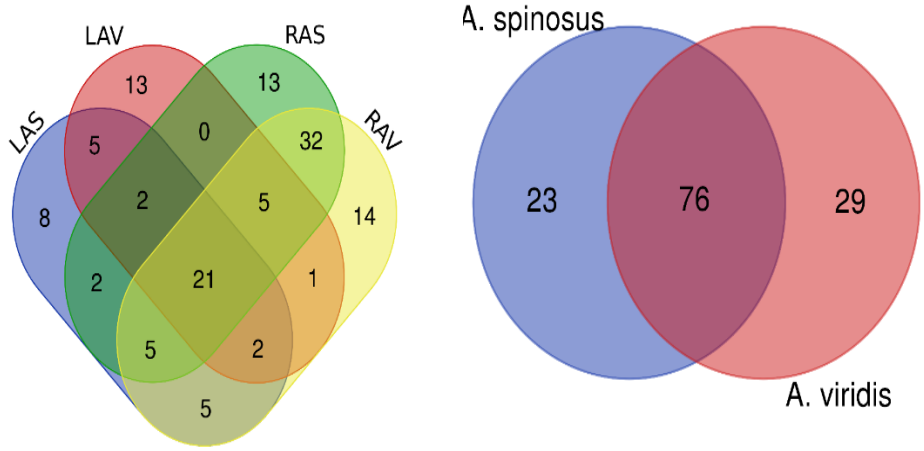


A B

**Figure 8.** Venn diagram illustrating the distribution metabolites. (A) Comparison of compounds between different plant organs (leaf and root) within each species. (B) Comparison of shared and unique compounds between the two *Amaranthus* species

**Table 2** the 48 distinct compounds from leaves and roots *A. spinosus* and *A. viridis* species based on Venn diagram analysis

| No | Copound | Part | CID/ ChemSpider ID | Molecular formula | Class |
|---|---|---|---|---|---|
| 1. | N-Acetylanthranilic Acid | LAS | 6971 | $C_9H_9NO_3$ | Acid |
| 2. | Lignocerylserotonin* | | 156122 | $C_{34}H_{58}N_2O_2$ | Lipid and derivates |
| 3. | Benzoic Acid | | 1094891 | $C_{19}H_{17}NO_7S$ | Lipid and derivates |
| 4. | Octadecanamide | | 594460 | $C_{28}H_{46}N_2O_2$ | Acid |
| 5. | Adonixanthin | | 16061189 | $C_{40}H_{54}O_3$ | Lipid and derivates |
| 6. | Juniperic acid | | 10466 | $C_{16}H_{32}O_3$ | Terpenoid |
| 7. | Sebacic acid | | 5192 | $C_{10}H_{18}O_4$ | Acid |
| 8. | Piperine | | 638024 | $C_{17}H_{19}NO_3$ | Alkaloid |
| 9. | Phaseolic acid 1 | LAV | 5281786 | $C_{13}H_{12}O_8$ | Lipid and derivates |
| 10. | Mesaconic Acid | | 638129 | $C_5H_6O_4$ | Acid |
| 11. | N-Palmitoyl Valine | | 11348810 | $C_{21}H_{41}NO_3$ | Amino acid |
| 12. | TEMPO | | 2724126 | $C_9H_{18}NO$ | Lipid and derivates |
| 13. | N-Acetylalanine | | 88064 | $C_5H_9NO_3$ | Amino acid |
| 14. | DL-Carnitine | | 288 | $C_7H_{15}NO_3$ | Acid |
| 15. | Heptanoic Acid | | 5283058 | $C_{22}H_{38}O_5$ | Vitamin |
| 16. | DL-Tyrosine | | 1153 | $C_9H_{11}NO_3$ | Terpenoid |
| 17. | Allantoic Acid/Allantoate | | 5287444 | $C_4H_7N_4O_4^-$ | Phenolic |
| 18. | Hydroxydecanoic Acid | | 56936290 | $C_{22}H_{40}O_{11}$ | Glycolipid |
| 19. | Undecatetrane | | 4656047 | $C_{14}H_{22}$ | Acid |
| 20. | N-Palmitoyl Alanine | | 14961184 | $C_{19}H_{37}NO_3$ | Vitamin |
| 21. | Beta-Damascenone | | 5366074 | $C_{13}H_{18}O$ | Acid |
| 22. | Isoferulic acid | RAS | 736186 | $C_{10}H_{10}O_4$ | Acid |
| 23. | Octadecanoic Acid | | 45359277 | $C_{18}H_{36}O_5$ | Acid |
| 24. | Succinic acid semialdehyde | | 1112 | $C_4H_6O_3$ | Amino acid |
| 25. | Indoleacetylglycine/acetic acid | | 440806 | $C_{12}H_{12}N_2O_4$ | Antioxidant |
| 26. | Hexadecanoic Acid | | 441449 | $C_{16}H_{32}O_4$ | Amino acid |
| 27. | Boc-Glycine | | 78288 | $C_7H_{13}NO_4$ | Amines |
| 28. | Phenyllactic Acid | | 1303 | $C_9H_{10}O_3$ | Lipid and derivates |
| 29. | Pentanorvitamin D3 | | 9547499 | $C_{29}H_{40}O_2$ | Amino acid |

| No | Copound | Part | CID/ ChemSpider ID | Molecular formula | Class |
|---|---|---|---|---|---|
| 30. | Ursolic Acid | | 64945 | $C_{30}H_{48}O_3$ | Acid |
| 31. | Dihydrocapsaicin | | 107982 | $C_{18}H_{29}NO_3$ | Lipid and derivates |
| 32. | L-Aspartate/ aspartic acid | | 5960 | $C_4H_7NO_4$ | Terpenoid |
| 33. | Hexanoic Acid | | 14490 | $C_6H_{12}O_3$ | Amino acid |
| 34. | 25-Dihydroxyvitamin D3 | | 9547502 | $C_{29}H_{42}O_4$ | Terpenoid |
| 35. | 27-Norvitamin D3 | RAV | 9547284 | $C_{26}H_{39}F_3O_2$ | Vitamin |
| 36. | Aconitic Acid | | 444212 | $C_6H_6O_6$ | Acid |
| 37. | Tetradecadienedioic acid | | 10405119 | $C_{18}H_{30}O_6$ | Lipid and derivate |
| 38. | Phosphatidic Acid | | 446066 | $C_{35}H_{69}O_8P$ | Lipid and derivates |
| 39. | L-Proline | | 80817 | $C_{11}H_{20}N_2O_3$ | Amino acid |
| 40. | Oleic Acid | | 445639 | $C_{18}H_{34}O_2$ | Lipid and derivates |
| 41. | L-α-Asparagine | | 6267 | $C_{32}H_{31}N_3O_7$ | Amino acid |
| 42. | Phenaceturic acid | | 68144 | $C_{10}H_{11}NO_3$ | Acid |
| 43. | L-Hydroxyproline | | 5810 | $C_5H_9NO_3$ | Amino acid |
| 44. | Petroselinic Acid | | 5281125 | $C_{18}H_{34}O_2$ | Lipid and derivates |
| 45. | NONIOSIDE D | | 10741757 | $C_{18}H_{32}O_{12}$ | Glycoside |
| 46. | Gentisic Acid | | 3469 | $C_7H_6O_4$ | Acid |
| 47. | Decanoic acid | | 16061039 | $C_{10}H_{17}NO_4$ | Lipid and derivates |
| 48. | β-Alanine diacetic acid | | 535795 | $C_7H_{11}NO_6$ | Other compound |

**Note:** * compound with ChEBI ID sources

## In Silico Analysis Prediction

### Biological Activity Prediction as Antidiabetic

Utilizing PASSonline, a researcher may predict the biological activity of specified substances. This study is valuable, particularly in early-stage pharmacological and phytochemical research, because it is less expensive, faster, and more ethical [16-18]. However, using this web server still requires experimental confirmation. A total of 48 distinct metabolites revealed diverse antidiabetic activities with Pa values (Figure 9). Adonixanthin, ursolic acid, and phenyllactic acid in LAS RAS samples, as well as DL-carnitine and gentisic acid in LAV RAV samples, had a high Pa value for almost all bioactivity parameters. This result was relevant to previous studies on antioxidants, glucose metabolism modulation (enhancing uptake, storage, and oxidation), and insulin sensitivity improvement [64-66]. Ursolic acid (triterpenoid) is mediated through multiple mechanisms such as inhibiting α-amylase, α-glucosidase, aldose reductase, and glycogen synthase kinase-3 enzymes [65, 67].

## Toxicity Analysis Prediction

### Acute Oral and Organ Toxicity Prediction Obtained by Protox-3.0 Web Server Analysis Prediction

The implication of the ProTox 3.0 web server is that detailed toxicity and mechanistic risk information can be obtained rapidly from structure alone, supporting safer chemical and drug design, earlier risk flagging, and reduced reliance on animal testing—while still requiring experimental validation for regulatory decisions [19]. Figure 10 shows the ProTox-3.0 analysis, which predicts acute oral toxicity with $LD_{50}$ values ranging from highly toxic (1 mg/kg, Class 1) to non-toxic (10,000 mg/kg, Class 6). The toxicity of pentanorvitamin $D_3$ and 25-dihydroxyvitamin $D_3$ in RAS *A. spinosus* leads to excessive levels of vitamin D along with insufficiency, increasing the probability of degenerative diseases such as diabetes [68]. DL-carnitine, L-α-asparagine, NONIOSIDE D, and decanoic acid are safe for LAV and RAV *A. viridis*, with varied toxicity depending on structure [69, 70].

Hepatotoxicity prediction assumes long-term (subchronic) effects influenced by specific metabolic pathways in the liver [71]. The prediction classifies benzoic acid, ursolic acid, piperine, and heptanoic acid (LAS, RAS, and RAV) as active in the liver, indicating potential hepatic effects despite their moderate $LD_{50}$ values (5000, 2000, and 1190 mg/kg) (Figure 11). These predictions are associated with hepatic metabolic mechanisms and pathways that influence bioactivation and compound toxicity potential [72-74].

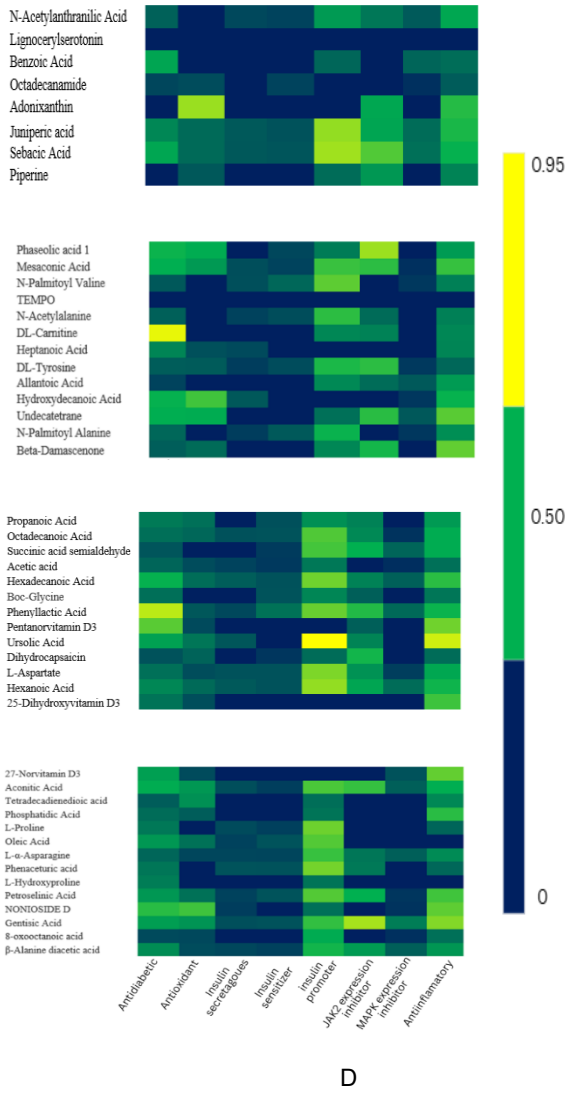


**Figure 9.** Prediction of antidiabetic activity via PASSonline analysis for phytochemical compounds identified in different organs of *A. spinosus* and *A. viridis*. (A) leaf of *A. spinosus* (LAS), (B) leaf of *A. viridis* (LAV), (C) root of *A. spinosus* (RAS), and (D) root of *A. viridis* (RAV).

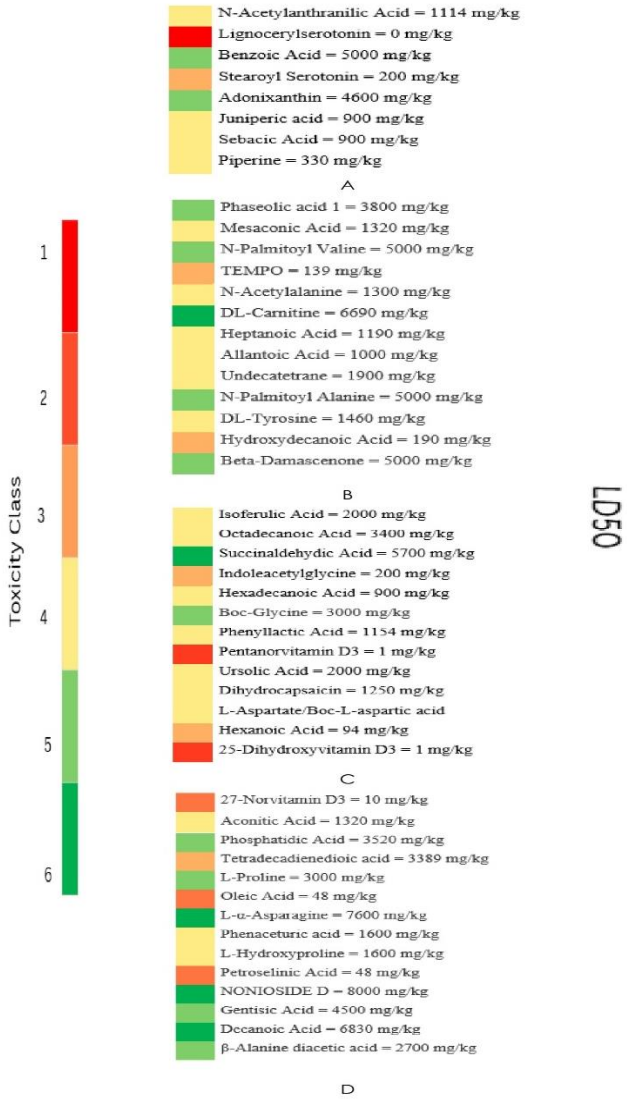


**Figure 10.** Toxicity prediction using Protox 3.0 for phytochemical compounds identified in different organs of *A. spinosus* and *A. viridis*. The predicted acute oral toxicity ($LD_{50}$ in mg/kg) is displayed for compounds from (A) *A. spinosus* leaves (LAS), (B) *A. viridis* leaves (LAV), (C) *A. spinosus* roots (RAS), and (D) *A. viridis* roots (RAS).

## Toxicological Endpoints Predicted Activity and Tox21 Nuclear Receptor Signaling Pathways

The evaluation of toxicological profiles across different endpoints showed that ursolic acid, dihydrocapsaicin, undecatrane, and β-alanine diacetic acid in LAV, RAS, and RAV were predicted to exhibit potential carcinogenic effects attributed to their molecular similarities, chemical fragment properties, and ability to interact with toxicological targets (Figure 11) [77, 76], despite some biological literature reporting therapeutic or anticancer effects for these compounds [77, 78]. Moreover, dihydrocapsaicin has mutagenic potential.

Nutritional toxicity was predicted activation for Boc-glycine, ursolic acid, dihydrocapsaicin, L-aspartate, 25-dihydroxyvitamin D3, 27-norvitamin D3, and L-hydroxyproline in LAS, RAS, and RAV, suggesting potential disturbances in nutrient absorption at excessive doses. Fatty acids such as octadecanoic acid,

oleic acid, and petroselinic acid demonstrated PPARγ activation, which is expected because they are lipid signalling modulators [79, 80]. Interestingly, polar amino acids, L-α-asparagine/L-asparagine, exhibited a PPAR-γ activation of 99%, which is remarkably higher than that of common fatty acids. However, these findings require further investigation [80].

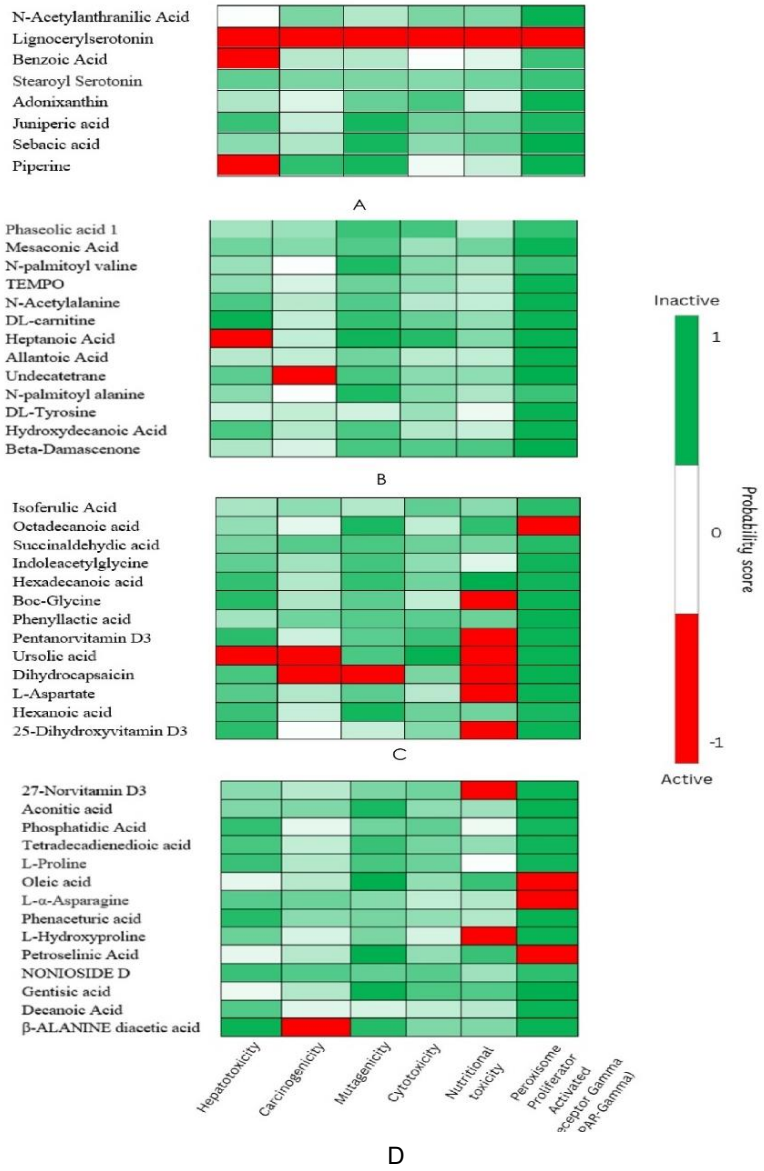


**Figure 11.** Protox 3.0 analysis predicted toxicity for phytochemical compounds identified in leaves and roots of *A. spinosus* and *A. viridis*. (A) LAS; (B) LAV; (C) RAS; and (D) RAV. The coloured box illustrates the different activity of the substances, with green indicating inactive, and red indicating active

## SwissADME Prediction

SwissADME is significant in early-stage drug discovery, allowing researchers to examine absorption, distribution, metabolism, and excretion (ADME) properties of many compounds without requiring physical samples [16]. This study supports the pre-filtration of compound collections by identifying molecules that are unable to exhibit beneficial drug-like qualities, and it contributes to the subsequent priority setting of screening results by analyzing ADME features of possible drug candidates. This facilitates the selection of molecules with a higher probability of becoming viable drug candidates [16, 17].

Based on this analysis of 48 metabolites from the leaves and roots of *A. spinosus* and *A. viridis*, it was found that the majority of the compounds tested met Lipinski's Rule of Five (RO5) criteria (Table 3).

However, there are several compounds that violate these rules, such as Lignocerylserotonin, which has a MW of 526.8 g/mol and a cLogP value of 6.77 in the LAS sample; Hydroxydecanoic Acid, which has HBD 6 and HBA 11 in the LAV sample; Phosphatidic acid, which has a BM of 648.9 g/mol and a cLogP of 9.36; and Nonioside D, which has an HBD of 7 and an HBA of 12 in the RAV sample, exceeding the ideal limits of BM 500 g/mol, lipophilicity (<5), HBD <5, and HBA <10 [16, 17]. These four compounds are a group of glycosides, glycolipids, lipids, and their derivatives that have long carbon chains. These conditions supported highly nonpolar and hydrophobic substances, significantly increasing the lipophilicity [81, 82]. Therefore, Nonioside D has a sugar unit that acts as both an HBD and an HBA. A single glucose unit has 5 HBDs and 6 HBAs. Therefore, a glycoside with two or more sugar units would easily exceed the HBD > 5 and HBA > 10 thresholds [16, 83].

**Table 3.** Lipinski's molecular descriptors for 48 distinct metabolites from leaves and roots *A. spinosus* and *A. viridis* using SwissADME analysis

| No | Copound | Part | MW (≤500) (g/mol) | HBD (≤5) | HBA (≤10) | cLog P (<5) | MR (≤10) | n-ROTB (≤10) | TPSA (Å²) |
|---|---|---|---|---|---|---|---|---|---|
| 1. | N-Acetylanthranilic Acid | LAS | 179,17 | 2 | 3 | 1.23 | 47.71 | 3 | 66.4 |
| 2. | Lignocerylserotonin* | | 526.8 | 0 | 2 | 6.77 | 170.80 | 6 | 40.62 |
| 3. | Benzoic Acid | | 403,4 | 2 | 7 | 2.67 | 101.34 | 7 | 131.29 |
| 4. | Octadecanamide | | 442.7 | 3 | 2 | 7.16 | 139.62 | 20 | 65.12 |
| 5. | Adonixanthin | | 582,9 | 2 | 3 | 1.23 | 186,96 | 10 | 57.53 |
| 6. | Juniperic acid | | 272,42 | 2 | 3 | 4.30 | 81.96 | 15 | 57.53 |
| 7. | Sebacic acid | | 202,25 | 2 | 4 | 1.88 | 53.73 | 9 | 74.6 |
| 8. | Piperine | | 285,34 | 0 | 3 | 3.03 | 85.47 | 4 | 38.77 |
| 9. | Phaseolic acid 1 | LAV | 296.23 | 4 | 8 | 0.38 | 69.44 | 7 | 141.36 |
| 10. | Mesaconic Acid | | 130.1 | 2 | 4 | -0.04 | 29.22 | 2 | 74.6 |
| 11. | N-Palmitoyl Valine | | 355.6 | 2 | 3 | 5.58 | 107.83 | 18 | 66.4 |
| 12. | TEMPO | | 156.25 | 0 | 2 | 0.57 | 49.78 | 0 | 3.24 |
| 13. | N-Acetylalanine | | 131.13 | 2 | 3 | -0.33 | 30.92 | 3 | 66.4 |
| 14. | DL-Carnitine | | 161.2 | 1 | 3 | -2.4 | 39.13 | 4 | 60.36 |
| 15. | Heptanoic Acid | | 382.5 | 3 | 5 | 3.65 | 109.32 | 13 | 94.83 |
| 16. | DL-Tyrosine | | 181.19 | 3 | 4 | -0.49 | 47.52 | 3 | 83.55 |
| 17. | Allantoic Acid/Allantoate | | 175.12 | 4 | 4 | -2.45 | 33.37 | 5 | 150.37 |
| 18. | Hydroxydecanoic Acid | | 480.5 | 6 | 11 | 0.38 | 115.56 | 12 | 175.37 |
| 19. | Undecatetrane | | 190.32 | 0 | 0 | 4.62 | 67.52 | 4 | 0 |
| 20. | N-Palmitoyl Alanine | | 327.5 | 2 | 3 | 4.92 | 98.22 | 17 | 66.4 |
| 21. | Beta-Damascenone | | 190.28 | 0 | 1 | 3.12 | 61.01 | 2 | 17.07 |
| 22. | Isoferulic acid | RAS | 194.18 | 2 | 7 | 0.85 | 61.51 | 6 | 118.51 |
| 23. | Octadecanoic Acid | | 332,5 | 4 | 5 | 3.26 | 93.9 | 16 | 97.99 |
| 24. | Succinic acid semialdehyde | | 102,09 | 1 | 1 | -0.17 | 23.31 | 3 | 54.37 |
| 25. | Indoleacetylglycine/acetic acid | | 248.23 | 4 | 4 | 0.49 | 64.48 | 5 | 102.42 |
| 26. | Hexadecanoic Acid | | 288,42 | 3 | 4 | 3.32 | 83.12 | 15 | 77.76 |
| 27. | Boc-Glycine | | 175.18 | 2 | 4 | 0.50 | 42.05 | 5 | 75.63 |
| 28. | Phenyllactic Acid | | 166,17 | 2 | 3 | 1.02 | 43.96 | 3 | 57.53 |
| 29. | Pentanorvitamin D3 | | 420,6 | 2 | 2 | 0.50 | 131.62 | 4 | 40.46 |
| 30. | Ursolic Acid | | 456,7 | 2 | 3 | 5.93 | 136.91 | 1 | 57.53 |
| 31. | Dihydrocapsaicin | | 307.4 | 2 | 3 | 3.70 | 90.99 | 11 | 58.56 |
| 32. | L-Aspartate/ aspartic acid | | 133.1 | 3 | 6 | 0.18 | 53.43 | 7 | 112.93 |
| 33. | Hexanoic Acid | | 132,16 | 2 | 3 | 0.44 | 33.89 | 5 | 57.53 |
| 34. | 25-Dihydroxyvitamin D3 | | 454.6 | 3 | 4 | 3.70 | 134.15 | 4 | 73.22 |
| 35. | 27-Norvitamin D3 | RAV | 440,6 | 2 | 5 | -1.42 | 121.59 | 7 | 40.46 |
| 36. | Aconitic Acid | | 174,11 | 3 | 6 | -0.68 | 35.8 | 4 | 111.9 |
| 37. | Tetradecadienedioic acid | | 342,4 | 4 | 6 | 2.59 | 93.56 | 12 | 115.06 |
| 38. | Phosphatidic Acid | | 648,9 | 2 | 8 | 9.36 | 185.0 | 36 | 129.17 |
| 39. | L-Proline | | 228,29 | 2 | 4 | 0.04 | 64.37 | 5 | 83.63 |
| 40. | Oleic Acid | | 282,5 | 1 | 2 | 5.65 | 89.94 | 15 | 37.3 |
| 41. | L-α-Asparagine | | 132,12 | 3 | 4 | -2.22 | 28.73 | 3 | 106.41 |
| 42. | Phenaceturic acid | | 193.2 | 2 | 3 | 0.83 | 50.6 | 5 | 66.4 |
| 43. | L-Hydroxyproline | | 131.13 | 3 | 4 | -1.65 | 33.69 | 1 | 69.56 |
| 44. | Petroselinic Acid | | 282,5 | 1 | 2 | 5.7 | 89.94 | 15 | 37.3 |
| 45. | NONIOSIDE D | | 440,4 | 7 | 12 | -1.76 | 97.08 | 10 | 195.6 |
| 46. | Gentisic Acid | | 154,12 | 3 | 4 | 0.74 | 37.45 | 1 | 77.76 |
| 47. | Decanoic acid | | 215.1 | 2 | 5 | -0.47 | 53.83 | 8 | 92.92 |
| 48. | β-Alanine diacetic acid | | 205,1 | 3 | 7 | -1.42 | 43.97 | 7 | 115.14 |

Note: MW = Molecular weight; g/mol (range: <500); HBD = Hydrogen bond donor (range:≤5); HBA = Hydrogen bond acceptor (range: ≤10); cLogP = High lipophilicity (expressed as LogP, range: <5); MR = Molar refractivity (range: 40–130); n-ROTB: number of rotatable bounds; TPSA = Topological polar surface area; Å2. *Denotes violation of Lipinski's RO5.

## Molecular Docking

Molecular docking is a simulation technique in computation that predicts the most ideal interaction response between small compounds (ligands) and active sites of protein targets in 3D structures (proteins, DNA, or RNA) with the objective to interpret fundamental chemical reactions at the molecular level [16]. This analysis was used in this study to predict the interaction and binding energy of *A. spinosus* and *A. viridis* leaf and root compounds with the protein involved in DM, cyclooxygenase-2 (COX-2, PDB ID: 1PXX). The expression of this protein increases significantly when influenced by cytokines, hyperglycemia, oxidative stress, and other inflammatory stimuli, causing increased inflammation, metabolic abnormalities, and tissue damage in people with diabetes [16, 84].

Table 4 showed the binding energy and RMSD (Root-Mean-Square Deviation) interaction between LAS, LAV, RAS, and RAV compounds from *A. spinosus* and *A. viridis*. Binding energy is one of the important parameters used in molecular docking analysis. This parameter provides information on the bond energy value to predict the affinity of complex bonds in determining the best compound that interacts with COX-2. The bond value displayed is positive, which leads to bond destabilization, and negative, which indicates complex bond stabilization [85]. Table 4 presents the results of all binding energy values that are either negative or stable, which are advantageous for the active site of the COX-2 target protein. The analyzed samples reveal multiple substances in the lowest binding energies: benzoic acid (-9.1 kcal/mol), adonixanthin (-9.2 kcal/mol), and piperine (-8.8 kcal/mol) in LAS; heptanoic acid (-8.1 kcal/mol) in LAV; indoleacetylglycine/acetic acid (-7.8 kcal/mol), pentanorvitamin D3 (-8.9 kcal/mol), ursolic acid (-9.7 kcal/mol), and 25-Dihydroxyvitamin D3 (-10.1 kcal/mol) in RAS; and 27-Norvitamin D3 (-7.7 kcal/mol) in RAV, compared to diclofenac (-7.5 kcal/mol) as a positive control. Previous research has shown that benzoic acid, ursolic acid, piperine, heptanoic acid, and 25-hydroxyvitamin D3 have antidiabetic, anti-inflammatory, and antioxidant properties by modulating and inhibiting the expression and signaling of various molecular targets, such as IR, IRS 1, Akt, GLUT4, AS160, IL 1β, TNF α, IFN γ, NF κB, STAT3/6, and the Akt/mTOR pathway [86-90].

Of all the interactions, the COX-2-25-Dihydroxyvitamin D3 complex showed the smallest binding energy value, indicating it as the best ligand. This is because the smaller the binding affinity value, the stronger the affinity of the bond and the more advantageous it is [...]. These results provide an understanding that the 25-Dihydroxyvitamin D3 compound from the RAS sample has the potential to be a candidate inhibitor of the COX-2 protein. However, further experimental studies are still needed.

Furthermore, the RMSD factor is useful for assessing position stability in molecular docking simulations since it represents the ordinary distance among atoms in the two contacting structures. The ideal RMSD value is ≤ 2.0 Å, 2–3 Å is acceptable, and ≥ 3 Å is incorrect [91]. The analysis results in Table 4 show that all RMSD values are 0, indicating that the simulations performed are valid.

**Table 4.** The binding energy of COX-2 protein with 44 compounds and Diclofenac from leaves and root *A. spinosus* and *A. viridis*

| No | Copound | Part | Binding energy (kcal/mol) | RMSD (Å) |
|---|---|---|---|---|
| 1. | N-Acetylanthranilic Acid | LAS | -6.6 | 0 |
| 2. | **Benzoic Acid** | | **-9.1** | **0** |
| 3. | Octadecanamide | | -7.4 | 0 |
| 4. | **Adonixanthin** | | **-9.2** | **0** |
| 5. | Juniperic acid | | -5.4 | 0 |
| 6. | Sebacic acid | | -5.8 | 0 |
| 7. | **Piperine** | | **-8.8** | **0** |
| 8. | Phaseolic acid 1 | LAV | -7.2 | 0 |
| 9. | Mesaconic Acid | | -5.3 | 0 |
| 10. | N-Palmitoyl Valine | | -6.1 | 0 |
| 11. | TEMPO | | -5.3 | 0 |
| 12. | N-Acetylalanine | | -5.6 | 0 |
| 13. | DL-Carnitine | | -5.3 | 0 |
| 14. | **Heptanoic Acid** | | **-8.1** | **0** |
| 15. | DL-Tyrosine | | -6.2 | 0 |
| 16. | Allantoic Acid/Allantoate | | -7.0 | 0 |
| 17. | Undecatetrane | | -7.3 | 0 |
| 18. | N-Palmitoyl Alanine | | -5.5 | 0 |
| 19. | Beta-Damascenone | | -6.3 | 0 |
| 20. | Isoferulic acid | RAS | -6.8 | 0 |

| No | Copound | Part | Binding energy (kcal/mol) | RMSD (Å) |
|---|---|---|---|---|
| 21. | Octadecanoic Acid | RAV | -6.4 | 0 |
| 22. | Succinic acid semialdehyde | | -4.4 | 0 |
| 23. | **Indoleacetylglycine/acetic acid** | | **-7.8** | **0** |
| 24. | Hexadecanoic Acid | | -5.5 | 0 |
| 25. | Boc-Glycine | | -5.8 | 0 |
| 26. | Phenyllactic Acid | | -6.3 | 0 |
| 27. | **Pentanorvitamin D3** | | **-8.9** | **0** |
| 28. | **Ursolic Acid** | | **-9.7** | **0** |
| 29. | Dihydrocapsaicin | | -6.9 | 0 |
| 30. | L-Aspartate/ aspartic acid | | -4.9 | 0 |
| 31. | Hexanoic Acid | | -5.0 | 0 |
| 32. | **25-Dihydroxyvitamin D3** | | **-10.1** | **0** |
| 33. | **27-Norvitamin D3** | | **-7.7** | **0** |
| 34. | Aconitic Acid | | -6.1 | 0 |
| 35. | Tetradecadienedioic acid | | -7.2 | 0 |
| 36. | L-Proline | | -6.1 | 0 |
| 37. | Oleic Acid | | -5.6 | 0 |
| 38. | L-α-Asparagine | | -5.4 | 0 |
| 39. | Phenaceturic acid | | -6.2 | 0 |
| 40. | L-Hydroxyproline | | -5.4 | 0 |
| 41. | Petroselinic Acid | | -5.1 | 0 |
| 42. | Gentisic Acid | | -6.7 | 0 |
| 43. | Decanoic acid | | -5.4 | 0 |
| 44. | β-Alanine diacetic acid | | -5.8 | 0 |
| 45. | Diclofenac | Positive control | -7.5 | 0 |

## Construction of the Hydrogen Bond among the COX-2 with Compounds based on Small Binding Energy

Hydrogen bond formation is another parameter required in molecular docking analysis because it is related to other parameters. The software used to visualize bond distances and numbers is BioVia Discovery Visualizer 2025. The ideal hydrogen bond distance is between 1.5 and 2.6 Å because the strength of the interaction is influenced by the bond distance. The longer the hydrogen bond distance formed (>3.0 Å), the smaller the bond affinity, so that the ligand-protein complex interaction becomes weaker and easier to break [92]. A single hydrogen bond has an energy of 20-25 kJ/mol when contributing to protein structure stability [93]. Table 5 shows the molecular docking results related to the number of hydrogen bonds formed that interact with residues in each complex analyzed.

The compound 25-Dihydroxyvitamin D3 interacts with the COX-2 protein with the smallest binding energy, forming four hydrogen bonds at the amino acid residues ASP229a, SER1143b, LEU224a, and ASN1375b with chains A and B at distances of 2.75, 3.44, 2.56, and 3.16, respectively. This is in contrast to diclofenac, which forms two hydrogen bonds at residues ARG2044c and GLY2045c on chain C at distances of 2.95 and 2.36 (Table 5 and Figure 12). Although the distance between hydrogen bonds in the diclofenac-COX-2 complex is smaller than in the 25-Dihydroxyvitamin D3-COX-2 complex, it should be noted that geometry (angle), number, stability during simulation, and other types of bonds that support it also influence the advantage of ligand-protein interaction [94]. Furthermore, when interacting with the target protein, the 25-Dihydroxyvitamin D3 compound binds to different chain residues (A and B) compared to the diclofenac compound, which binds only to chain B. Heteromer interactions form bond energy (free energy) that is almost always lower (more stable) in complete quaternary structures than in monomers. This makes the compound 25-Dihydroxyvitamin D3, which has potential as an antidiabetic agent through the inhibition of proteins involved in the inflammatory process by binding to amino acid residues from different chains.

**Table 5.** Hydrogen bond formation and interacting residues of COX-2 protein with each compound (small binding energy) that were analysed by Biovia Discovery Studio Visualizer 2019

| No | Copound | part | Interacting residues | No. of H-bond | H-bonded residue | Distance (Å) |
|---|---|---|---|---|---|---|
| **1.** | Benzoic Acid | LAS | PRO1153b, CYS1036b, **ASN1034b, MET1048b, SER1049b** | 3 | ASN1034b,<br>MET1048b,<br>SER1049b | 3.18<br>3.48<br>3.05 |
| **2.** | Adonixanthin | | CYS3036d, **GLY3045d, GLU3046D, ALA3156d** | 2 | GLY3045d<br>GLU3046D | 2.75<br>3.54 |
| **3.** | Piperine | | **ARG2044c, PRO2154c**, ALA2156c, VAL2155c, LEU2152c, ARG2469c | 2 | ARG2044c<br>PRO2154c | 3.19<br>3.72 |
| **4.** | Heptanoic Acid | LAV | CYS2047c, CYS2036c, PRO2153c, LYS2468c, GLN2024c, **ASN2043c, ARG2044c, GLN3543d, TYR2130c, CYS2041c** | 5 | ASN2043c<br>ARG2044c<br>GLN3543d<br>TYR2130c,<br>CYS2041c | 2.68<br>3.07<br>2.92<br>3.08<br>3.10 |
| **5.** | Indoleacetylglycine/acetic acid | RAS | PRO3154d, LEU3152d, ARG3469d, **PRO3153d, GLN3461d, GLY3045d, GLU3465d, CYS3036d** | 5 | PRO3153d<br>GLN3461d<br>GLY3045d<br>GLU3465d<br>CYS3036d | 2.56<br>2.95<br>2.89<br>2.33<br>2.99 |
| **6.** | Pentanorvitamin D3 | | ARG104b, PRO542a, PHE1371b, **TYR1122b** | 1 | TYR1122b | 3.22 |
| **7.** | Ursolic Acid | | **SER2143c, ASN2144c, GLU2140c** | 3 | SER2143c<br>ASN2144c<br>GLU2140c | 2.74<br>3.23<br>2.53 |
| **8.** | 25-Dihydroxyvitamin D3 | | LEU145a, **ASP229a, SER1143b, LEU224a, ASN1375b** | 4 | ASP229a<br>LEU224a<br>LEU224a<br>ASN1375b | 2.75<br>3.44<br>2.56<br>3.16 |
| **9.** | 27-Norvitamin D3 | RAV | TYR1136b, **ASN1034b, GLN327a, SER1049b, TRP323a, GLU322a**, ALA1156b | 5 | ASN1034b<br>GLN327a<br>SER1049b<br>TRP323a<br>GLU322a | 2.47<br>3.20<br>3.06<br>3.37<br>2.25 |
| **10.** | Diclofenac | Control | LEU2152c, CYS2047c, PRO2153c, **ARG2044c, GLY2045c** | 2 | ARG2044c,<br>GLY2045c | 2.95<br>2.36 |

Note: a = chain A; b = chain B, c = chain C, and d = chain D in protein target

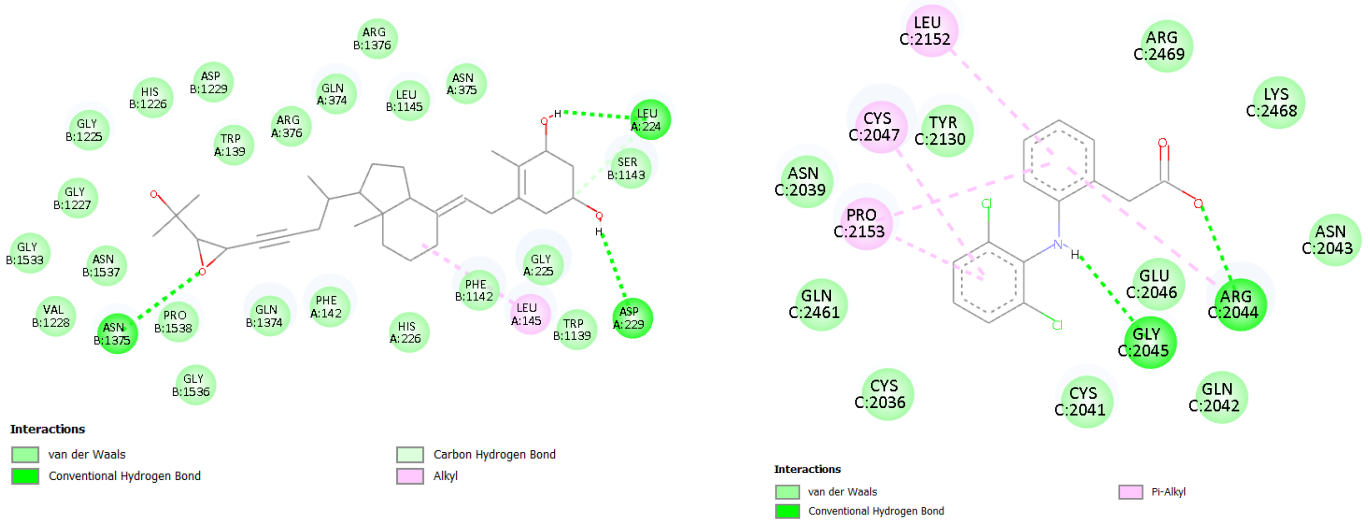


A B

**Figure 12.** Hydrogen bond formation and interacting residues of COX-2 protein from Biovia Discovery Studio Visualizer 2025 and A blue dash presents the hydrogen bond. A. 25-Dihydroxyvitamin D3-COX-2; B. Diclofenac-COX-2

## Conclusions

This study definitively establishes the effectiveness of the traditional food sources, *A. spinosus* and *A. viridis*, as significant antidiabetic nutraceutical candidates. Researchers used LC-HRMS and comprehensive chemometric analysis to accurately define the detailed, organ-specific metabolomic profiles of leaves and roots collected from Buru Island's Wallacea Areas, revealing unique metabolic pathways between aerial and subterranean tissues. Crucially, in silico predictions identified two key compounds with high antidiabetic activity and favorable toxicological profiles, including 25-Dihydroxyvitamin D3 and ursolic acid from the RAS sample, compared with the positive control (diclofenac) when interacting with the COX-2 protein involved in diabetes. The heavy interaction is supported by many interaction types, such as hydrogen bonds and hydrophobic contacts in the active side of the COX-2 protein. However, the results of this activity are only predictions, requiring further study using molecular dynamics simulations to observe the dynamic interactions between proteins and ligands at the atomic level and to validate their inhibitory potential experimentally in order to obtain a comprehensive understanding of the activity of 25-Dihydroxyvitamin D3 compounds from RAS samples (*A. spinosus* roots). This study reveals that *Amaranthus* roots have considerable potential as nutraceutical and pharmaceutical candidates for diabetes management.

## Conflicts of Interest

The authors declare that there is no conflict of interest regarding the publication of this paper.

## Acknowledgment

We would like to thank Lembaga Pengelola Dana Pendidikan/LPDP for supporting the publication of this research article.

## References

[1] Jiménez-Aguilar, D. M., & Grusak, M. A. (2017). Minerals, vitamin C, phenolics, flavonoids and antioxidant activity of *Amaranthus* leafy vegetables. *Journal of Food Composition and Analysis, 58*, 33–39. https://doi.org/10.1016/j.jfca.2017.01.008.

[2] Sarker, U., Oba, S., Ullah, R., Bari, A., Ercisli, S., Skrovankova, S., Adamkova, A., Zvonkova, M., & Mlcek, J. (2024). Nutritional and bioactive properties and antioxidant potential of *Amaranthus tricolor*, *A. lividus*, *A. viridis*, and *A. spinosus* leafy vegetables. *Heliyon, 10*(9), e30453. https://doi.org/10.1016/j.heliyon.2024.e30453.

[3] Nkobole, N., & Gerhard, P. (2021). ¹H NMR and LC-MS-based metabolomics analysis of wild and cultivated *Amaranthus* spp. *Molecules, 26*(4), 795. https://doi.org/10.3390/molecules26040795.

[4] Abdel-Moez, G., Avula, B., Sayed, H., Khalifa, A., Ross, S., Katragunta, K., Khan, I., & Mohamed, S. (2023). Phytochemical profiling of three *Amaranthus* species using LC-MS/MS metabolomics approach and chemometric tools. *Journal of Pharmaceutical and Biomedical Analysis, 236*, 115722. https://doi.org/10.1016/j.jpba.2023.115722.

[5] Zhan, X., Chen, Z., Chen, R., & Shen, C. (2022). Environmental and genetic factors involved in plant protection-associated secondary metabolite biosynthesis pathways. *Frontiers in Plant Science, 13*, 877304. https://doi.org/10.3389/fpls.2022.877304.

[6] Araujo-León, J., Pino, I., Ortíz-Andrade, R., Hidalgo-Figueroa, S., Carrera-Lanestosa, A., Brito-Argáez, L., González-Sánchez, A., Giácoman-Vallejos, G., Hernández-Abreu, O., Peraza-Sánchez, S., Xingú-López, A., & Aguilar-Hernández, V. (2024). HPLC-based metabolomic analysis and characterization of *Amaranthus cruentus* leaf and inflorescence extracts for their antidiabetic and antihypertensive potential. *Molecules, 29*, Article number not assigned. https://doi.org/10.3390/molecules29xxxx.

[7] Prince, M., Zihad, S., Ghosh, P., Sifat, N., Rouf, R., Shajib, G., Alam, M., Shilpi, J., & Uddin, S. (2021). *Amaranthus spinosus* attenuated obesity-induced metabolic disorders in high-carbohydrate-high-fat diet-fed obese rats. *Frontiers in Nutrition, 8*, 676744. https://doi.org/10.3389/fnut.2021.676744

[8] Sun, J., Liu, B., Rustiami, H., Xiao, H., Shen, X., & Peng, K. (2024). Mapping Asian plants: Plant diversity and a checklist of vascular plants in Indonesia. *Plants, 13*, Article number not assigned. https://doi.org/10.3390/plants13xxxx.

[9] Van Welzen, P. C., Parnell, J. A. N., & Slik, J. W. F. (2011). Wallace's line and plant distributions: Two or three phytogeographical areas and where to group Java? *Biological Journal of the Linnean Society, 103*(3), 531–545. https://doi.org/10.1111/j.1095-8312.2011.01647.x.

[10] Aryal, B., Adhikari, B., Aryal, N., Bhattarai, B. R., Khadayat, K., & Parajuli, N. (2021). LC-HRMS profiling and antidiabetic, antioxidant, and antibacterial activities of *Acacia catechu* (L.f.) Willd. *BioMed Research International, 2021*, 7588711. https://doi.org/10.1155/2021/7588711.

[11] Zengin, G., Nilofar, Yildiztugay, E., Bouyahya, A., Cavusoglu, H., Gevrenova, R., & Zheleva-Dimitrova, D. (2023). A comparative study on UHPLC-HRMS profiles and biological activities of *Inula sarana* different extracts and its beta-cyclodextrin complex. *Antioxidants, 12*(10), 1842. https://doi.org/10.3390/antiox12101842.
[12] Statistics Buru Regency (BPS). (2024). *Lolong Guba district in figures*. BPS-Statistics Buru Regency.
[13] Supriadi, A., Ridhowati, S., Saputra, D., Wulandari, W., & Lestari, S. D. (2025). Untargeted metabolomics profiling for the geographical authentication of traditional pempek using high-resolution orbitrap mass spectrometry. *Food Chemistry Advances, 6*, 100914. https://doi.org/10.1016/j.focha.2025.100914.
[14] Dadwal, V., Joshi, R., & Gupta, M. (2022). A comparative metabolomic investigation in fruit sections of *Citrus medica* L. and *Citrus maxima* L. using UHPLC-QTOF-IMS. *Food Research International, 157*, 111486. https://doi.org/10.1016/j.foodres.2022.111486.
[15] Daina, A., & Zoete, V. (2019). Application of the SwissDrugDesign online resources in virtual screening. *International Journal of Molecular Sciences, 20*(18), 4612. https://doi.org/10.3390/ijms20184612.
[16] Mohammed, A. E., Alghamdi, S. S., Shami, A., Suliman, R. S., Aabed, K., Alotaibi, M. O., & Rahman, I. (2023). In silico prediction of *Malvaviscus arboreus* metabolites and green synthesis of silver nanoparticles. *International Journal of Nanomedicine, 18*, 2141–2162. https://doi.org/10.2147/IJN.S401097.
[17] Selvakumaran, M., Imran, P. M., Kubaib, A., Azam, M., Basha, A. A., & Al-Resayes, S. I. (2024). Anti-inflammatory and antidiabetic activity of newly synthesized derivatives of 4AP2BOB. *Journal of Molecular Liquids, 396*, 123983. https://doi.org/10.1016/j.molliq.2023.123983
[18] Banerjee, P., Kemmler, E., Dunkel, M., & Preissner, R. (2024). ProTox 3.0: A webserver for the prediction of toxicity of chemicals. *Nucleic Acids Research, 52*(W1), W513–W520. https://doi.org/10.1093/nar/gkae347.
[19] Sadowska-Bartosz, I., & Bartosz, G. (2021). Biological properties and applications of betalains. *Molecules, 26*(9), 2520. https://doi.org/10.3390/molecules26092520.
[20] Martinez, R. M., Melo, C. P. B., Pinto, I. C., Mendes-Pierotti, S., Vignoli, J. A., Verri, W. A., & Casagrande, R. (2024). Betalains: A narrative review on pharmacological mechanisms supporting nutraceutical potential. *Foods, 13*(23), 3909. https://doi.org/10.3390/foods13233909.
[21] Wang, H., Wang, R., Harrison, S., & Prentice, I. C. (2022). Leaf morphological traits as adaptations to multiple climate gradients. *Journal of Ecology, 110*, 1344–1355. https://doi.org/10.1111/1365-2745.13870.
[22] Kreszies, T., Shellakkutti, N., Osthoff, A., Yu, P., Baldauf, J. A., Zeisler-Diehl, V. V., Ranathunge, K., Hochholdinger, F., & Schreiber, L. (2019). Osmotic stress enhances suberization of apoplastic barriers in barley seminal roots. *New Phytologist, 221*(1), 180–194. https://doi.org/10.1111/nph.15391.
[23] Grünhofer, P., Schreiber, L., & Kreszies, T. (2021). Suberin in monocotyledonous crop plants. In S. Mukherjee & F. Baluška (Eds.), *Rhizobiology: Molecular physiology of plant roots* (pp. xx–xx). Springer. https://doi.org/10.1007/978-3-030-XXXX-X.
[24] Chen, A., Liu, T., Wang, Z., & Chen, X. (2022). Plant roots suberin: A layer of defence against biotic and abiotic stresses. *Frontiers in Plant Science, 13*, 1056008. https://doi.org/10.3389/fpls.2022.1056008.
[25] Sarker, U., & Oba, S. (2019). Nutraceuticals, antioxidant pigments, and phytochemicals in the leaves of *Amaranthus spinosus* and *Amaranthus viridis*. *Scientific Reports, 9*, 20413. https://doi.org/10.1038/s41598-019-50923-5.
[26] Vazquez-Leon, L. A., Paramo-Calderon, D. E., Robles-Olvera, V. J., Valdés-Rodríguez, O. A., Pérez-Vázquez, A., García-Alvarado, M. A., & Rodríguez-Jimenes, G. C. (2017). Variation in bioactive compounds and antiradical activity of *Moringa oleifera* leaves. *European Food Research and Technology, 243*, 1593–1608. https://doi.org/10.1007/s00217-017-2876-0.
[27] Ciasa, B., Lanubile, A., Marocco, A., Pascale, M., Logrieco, A. F., & Lattanzio, V. M. T. (2020). Integrated open-source workflow for LC-HRMS plant metabolomics. *Frontiers in Plant Science, 11*, 111. https://doi.org/10.3389/fpls.2020.00111.
[28] Salam, U., Ullah, S., Tang, Z., Elateeq, A., Khan, Y., Khan, J., Khan, A., & Ali, S. (2023). Plant metabolomics: Roles of primary and secondary metabolites against environmental stress factors. *Life, 13*, Article number not assigned. https://doi.org/10.3390/life13xxxx.
[29] Zhang, Y., Huang, W., Zhang, C., Huang, H., Yang, S., Wang, Y., Huang, Z., Tang, Y., Li, X., Lian, H., Li, H., Zhang, F., & Sun, B. (2023). Variation in health-promoting compounds and antioxidant capacity of three leafy vegetables. *Molecules, 28*(12), 4780. https://doi.org/10.3390/molecules28124780.
[30] Gargallo-Garriga, A., Preece, C., Sardans, J., Oravec, M., Urban, O., & Peñuelas, J. (2018). Root exudate metabolomes change under drought. *Scientific Reports, 8*, 12655. https://doi.org/10.1038/s41598-018-30956-4.
[31] Nemadodzi, L. E., & Gudani, M. M. (2024). ^1H NMR-based metabolomics profile of green and red *Amaranthus* grown in open field versus greenhouse cultivation system. *Metabolites, 14*(1), 21. https://doi.org/10.3390/metabo14010021.
[32] Kar, A., & Bhattacharjee, S. (2022). Exploring polyphenol-based bioactive antioxidants of underutilized herb *Amaranthus spinosus* L. for medicinal purposes. *Journal of Exploratory Research in Pharmacology, 7*(3), 151–163.
[33] Lin, X. R., Yang, D., Wei, Y. F., Ding, D. C., Ou, H. P., & Yang, S. D. (2024). *Amaranthus* plants with various color phenotypes recruit different soil microorganisms in the rhizosphere. *Plants, 13*(16), 2200. https://doi.org/10.3390/plants13162200.

[34] Fouad, M. S., Ghareeb, M. A., Hamed, A. A., Schwaiger, S., Stuppner, H., Halabalaki, M., Amaral, J. G., & David, J. M. (2024). Exploring the antioxidant, anticancer, and antimicrobial potential of *Amaranthus viridis* L. collected from Fayoum Depression: Phytochemical and biological aspects. *South African Journal of Botany, 166*, 297–310. https://doi.org/10.1016/j.sajb.2024.01.021.
[35] Sampaio, B. L., Edrada-Ebel, R., & Da Costa, F. B. (2016). Effect of the environment on the secondary metabolic profile of *Tithonia diversifolia*: A model for environmental metabolomics of plants. *Scientific Reports, 6*, 29265. https://doi.org/10.1038/srep29265.
[36] Javed, M., Akram, M., Habib, N., Tanwir, K., Ali, Q., Niazi, N. K., Gul, H., & Iqbal, N. (2017). Deciphering the growth, organic acid exudations, and ionic homeostasis of *Amaranthus viridis* L. and *Portulaca oleracea* L. under lead chloride stress. *Environmental Science and Pollution Research, 25*, 2958–2971. https://doi.org/10.1007/s11356-017-0631-3.
[37] Aminu, M., & Ahmad, N. A. (2020). Complex chemical data classification and discrimination using locality preserving partial least squares discriminant analysis. *ACS Omega, 5*(41), 26601–26610. https://doi.org/10.1021/acsomega.0c03663.
[38] Hamany-Djande, C. Y., Piater, L. A., Steenkamp, P. A., Tugizimana, F., & Dubery, I. A. (2021). A metabolomics approach and chemometric tools for differentiation of barley cultivars and biomarker discovery. *Metabolites, 11*(9), 578. https://doi.org/10.3390/metabo11090578.
[39] Showemimo, F., Amira, J., Soyombo, M. R., & Porbeni, J. B. O. (2021). Trait selection criteria for genetic improvement of grain and leafy amaranth (*Amaranthus* spp.) using principal component analysis. *Egyptian Journal of Agricultural Research, 99*, 170–179.
[40] Yeshitila, M., Gedebo, A., Tesfaye, B., Tugizimana, F., & Dubery, I. A. (2023). Multivariate analysis for yield and yield-related traits of amaranth genotypes from Ethiopia. *Heliyon, 9*(7), e18207. https://doi.org/10.1016/j.heliyon.2023.e18207.
[41] Tan, W. N., Nagarajan, K., Lim, V., Azizi, J., Khaw, K.-Y., Tong, W. Y., Leong, C. R., & Chear, N. J. Y. (2022). Metabolomics analysis and antioxidant potential of endophytic *Diaporthe fraxini* ED2 grown in different culture media. *Journal of Fungi, 8*(5), 519. https://doi.org/10.3390/jof8050519.
[42] Li, R., Sun, Z., Zhao, Y., Li, L., Yang, X., Cen, J., Chen, S., Li, C., & Wang, Y. (2021). Application of UHPLC-Q-TOF-MS/MS metabolomics approach to investigate the taste and nutrition changes in tilapia fillets treated with different thermal processing methods. *Food Chemistry, 356*, 129737. https://doi.org/10.1016/j.foodchem.2021.129737.
[43] Windarsih, A., Rohman, A., Bakar, N. K. A., & Erwanto, Y. (2023). Metabolomics approach using LC-Orbitrap high-resolution mass spectrometry and chemometrics for authentication of beef meats from different origins in Indonesia. *Sains Malaysiana, 52*(10), 2869–2887.
[44] Yu, X., Wang, Y., Yan, X., Leng, T., Xie, J., Yu, Q., & Chen, Y. (2024). Metabolomics combined with correlation analysis revealed the differences in antioxidant activities of lotus seeds with varied cultivars. *Foods, 13*(7), 1084. https://doi.org/10.3390/foods13071084.
[45] Adhikari, B. (2021). Roles of alkaloids from medicinal plants in the management of diabetes mellitus. *Journal of Chemistry, 2021*, 20909063. https://doi.org/10.1155/2021/20909063.
[46] Surowiak, A. K., Balcerzak, L., Lochyński, S., & Strub, D. J. (2021). Biological activity of selected natural and synthetic terpenoid lactones. *International Journal of Molecular Sciences, 22*(9), 5036. https://doi.org/10.3390/ijms22095036.
[47] Behl, T., Gupta, A., Albratty, M., Najmi, A., Meraya, A. M., Alhazmi, H. A., Anwer, M. K., Bhatia, S., & Bungau, S. G. (2022). Alkaloidal phytoconstituents for diabetes management: Exploring the unrevealed potential. *Molecules, 27*(18), 5851. https://doi.org/10.3390/molecules27185851.
[48] Ogawa, E., Suzuki, N., Kamiya, T., & Hara, H. (2024). Sebacic acid, a royal jelly-containing fatty acid, decreases LPS-induced IL-6 mRNA expression in differentiated human THP-1 macrophage-like cells. *Journal of Clinical Biochemistry and Nutrition, 74*(3), 192–198. https://doi.org/10.3164/jcbn.23-78.
[49] Haq, I. U., Imran, M., Nadeem, M., Tufail, T., Gondal, T. A., & Mubarak, M. S. (2021). Piperine: A review of its biological effects. *Phytotherapy Research, 35*(2), 680–700. https://doi.org/10.1002/ptr.6855.
[50] Liu, G., Qin, P., Cheng, X., Wu, L., Wang, R., & Gao, W. (2023). Ursolic acid: Biological functions and application in animal husbandry. *Frontiers in Veterinary Science, 10*, 1251248. https://doi.org/10.3389/fvets.2023.1251248.
[51] Wang, J., Cui, J., Liu, Z., Yang, Y., Li, Z., & Liu, H. (2024). Untargeted metabolomics based on ultra-high-performance liquid chromatography coupled with quadrupole Orbitrap high-resolution mass spectrometry for differential metabolite analysis of *Pinelliae Rhizoma* and its adulterants. *Molecules, 29*(9), 2155. https://doi.org/10.3390/molecules29092155.
[52] Correnti, S., Fanelli, G., Preianò, M., Lelli, V., Tarantino, M., Fregola, A., Bitonti, M., Chiarella, E., Timperio, A. M., Rinalducci, S., Savino, R., & Terracciano, R. (2025). Untargeted metabolomics fingerprints in seminal plasma of patients with abnormal sperm morphology using high-performance liquid chromatography and mass spectrometry. *Frontiers in Molecular Biosciences, 12*, 1578998. https://doi.org/10.3389/fmolb.2025.1578998.
[53] Osmolovskaya, N., Bilova, T., Gurina, A., Orlova, A., Vu, V. D., Sukhikh, S., Zhilkina, T., Frolova, N., Tarakhovskaya, E., Kamionskaya, A., & Frolov, A. (2025). Metabolic responses of *Amaranthus caudatus* roots and leaves to zinc stress. *Plants, 14*(14), 2119. https://doi.org/10.3390/plants14142119.
[54] Song, W., Wei, Q., Shi, Z., Pan, Y., Li, Z., & Wang, F. (2025). Integrating transcriptome and metabolomics revealed the key metabolic pathway response of *Amaranthus retroflexus* L. to resistance to fomesafen. *PLOS ONE, 20*(2), e0312198. https://doi.org/10.1371/journal.pone.0312198.
[55] Siamey, J., Amissah, J. N., Ofori, P. A., Amoah, R. A., Mensah, E. O., & Kotey, D. A. (2025). Agro-morphological and molecular characterization of *Amaranthus* genotypes. *PLOS ONE, 20*(9),

e0328567. https://doi.org/10.1371/journal.pone.0328567.
[56] Chen, A., Liu, T., Wang, Z., & Chen, X. (2022). Plant root suberin: A layer of defence against biotic and abiotic stresses. *Frontiers in Plant Science, 13*, 1056008. https://doi.org/10.3389/fpls.2022.1056008.
[57] Mehravi, S., Hanifei, M., Gholizadeh, A., & Khodadadi, M. (2023). Water deficit stress changes in physiological, biochemical, and antioxidant characteristics of anise (*Pimpinella anisum* L.). *Plant Physiology and Biochemistry, 201*, 107806. https://doi.org/10.1016/j.plaphy.2023.107806.
[58] Hajib, A., El Harkaoui, S., Choukri, H., Khouchlaa, A., Aourabi, S., El Menyiy, N., Bouyahya, A., & Matthaeus, B. (2023). Apiaceae family: An important source of petroselinic fatty acid—Abundance, biosynthesis, chemistry, and biological properties. *Biomolecules, 13*(11), 1675. https://doi.org/10.3390/biom13111675.
[59] Swarnakumari, S., Mohan, S., Sasikala, M., & Umapoorani, T. (2021). Comparative studies on *Amaranthus viridis* and *Amaranthus spinosus*. *International Journal of Pharmaceutical Sciences and Research, 12*(10), 5618–5623.
[60] Sümengen Özdenefe, M., Büyükkaya Kayış, F., Erol, Ü. H., & Mercimek Takcı, A. (2024). Phytochemical screening and in vitro biological activity of *Amaranthus viridis* growing in Northern Cyprus. *International Journal of Secondary Metabolite, 11*(3), 592–603.
[61] Hosseini, R., & Heidari, M. (2025). Impact of drought stress on biochemical and molecular responses in lavender (*Lavandula angustifolia* Mill.): Effects on essential oil composition and antibacterial activity. *Frontiers in Plant Science, 16*, Article 1405497. https://doi.org/10.3389/fpls.2025.1506660.
[62] Leitão, A. M. F., Silva, B. R., Barbalho, E. C., Paulino, L. R. M., Costa, F. das C., Martins, F. S., & Silva, J. R. V. (2024). The role of L-carnitine in the control of oxidative stress and lipid β-oxidation during in vitro follicle growth, oocyte maturation, embryonic development, and cryopreservation: A review. *Zygote, 32*(5), 335–340. https://doi.org/10.1017/S096719942400039X.
[63] Sundaresan, A., Radhiga, T., & Pugalendi, K. V. (2016). Ursolic acid and rosiglitazone combination improves insulin sensitivity by increasing skeletal muscle insulin-stimulated IRS-1 tyrosine phosphorylation in high-fat diet-fed C57BL/6J mice. *Journal of Physiology and Biochemistry, 72*, 345–352.
[64] Razliqi, R. N., Ahangarpour, A., Mard, S. A., & Khorsandi, L. (2023). Gentisic acid ameliorates type 2 diabetes induced by nicotinamide–streptozotocin in male mice by attenuating pancreatic oxidative stress and inflammation through modulation of Nrf2 and NF-κB pathways. *Life Sciences, 325*, 121770. https://doi.org/10.1016/j.lfs.2023.121770.
[65] Ahirwar, P., & Malik, J. K. (2021). Mechanistic insight into the antidiabetic potential of ursolic acid: *In silico* molecular docking. *Middle East Research Journal of Pharmaceutical Sciences, 1*(1), 12–23.
[66] Marcinowska-Suchowierska, E., Kupisz-Urbańska, M., Łukaszkiewicz, J., Płudowski, P., & Jones, G. (2018). Vitamin D toxicity: A clinical perspective. *Frontiers in Endocrinology, 9*, 550. https://doi.org/10.3389/fendo.2018.00550.
[67] Jurowski, K., & Frydrych, A. (2025). First toxicity profile of aminoindane-based new psychoactive substances: 2-aminoindane (2-AI, CAS: 2975-41-9) and N-methyl-2-aminoindane (NM-2-AI, CAS: 24445–44–1)—Comprehensive prediction of toxicological endpoints important from a clinical and forensic perspective using *in silico* multi-approach. *Toxicology in Vitro, 110*, 106149.
[68] Zhi, H., Wang, Z., Zhu, X., Wu, W., Yang, L., Dai, Y., Wang, Z., Jiang, L., Tan, Y., Liu, X., & Liu, L. (2025). Chronic liver injury decreases levels of cerebral carnitine and acetylcarnitine in rats partly due to downregulation of organic cation transporters OCT1/2 and OCTN2 at the blood–brain barrier. *Drug Metabolism and Disposition, 53*(5), 100072. https://doi.org/10.1124/dmd.124.100072.
[69] Yu, K. N., Nadanaciva, S., Rana, P., Lee, D. W., Ku, B., Roth, A. D., Dordick, J. S., Will, Y., & Lee, M. Y. (2018). Prediction of metabolism-induced hepatotoxicity on three-dimensional hepatic cell culture and enzyme microarrays. *Archives of Toxicology, 92*(3), 1295–1310. https://doi.org/10.1007/s00204-018-2199-1.
[70] Jurowski, K., & Kobylarz, D. (2025). Toxicity assessment of the novel psychoactive substance HU-210 (Hebrew University 210; CAS: 112830–95–2): First insight into toxicophores and critical toxicity parameters using *in silico* methods for clinical and forensic toxicology. *Toxicology Letters, 410*, 39–57.
[71] Biswas, S., Kar, A., Sharma, N., Haldar, P. K., & Mukherjee, P. K. (2021). Synergistic effect of ursolic acid and piperine in $CCl_4$-induced hepatotoxicity. *Annals of Medicine, 53*(1), 2009–2017. https://doi.org/10.1080/07853890.2021.1986284.
[72] Khwaza, V., Oyedeji, O. O., & Aderibigbe, B. A. (2020). Ursolic acid-based derivatives as potential anticancer agents: An update. *International Journal of Molecular Sciences, 21*(16), 5920. https://doi.org/10.3390/ijms21165920.
[73] Risangud, N., Jangpromma, N., Kunnaja, P., Chiranthanut, N., Daduang, S., Chansaenpak, K., & Yubolphan, R. (2025). Enhancing the therapeutic efficacy of piperine in colorectal cancer: Development and evaluation of piperine-loaded PLGA-b-PEG copolymer nanoparticles. *European Journal of Pharmaceutics and Biopharmaceutics*, 114796. https://doi.org/10.1016/j.ejpb.2025.114796.
[74] Mitra, S., Anand, U., Jha, N. K., Shekhawat, M. S., Saha, S. C., Nongdam, P., Rengasamy, K. R. R., Proćków, J., & Dey, A. (2022). Anticancer applications and pharmacological properties of piperidine and piperine: A comprehensive review on molecular mechanisms and therapeutic perspectives. *Frontiers in Pharmacology, 12*, 772418. https://doi.org/10.3389/fphar.2021.772418.
[75] Chauhan, A., Pathak, V. M., Yadav, M., Chauhan, R., Babu, N., Chowdhary, M., Ranjan, A., Mathkor, D. M., Haque, S., Tuli, H. S., Ramniwas, S., & Yadav, V. (2024). Role of ursolic acid in preventing gastrointestinal cancer: Recent trends and future perspectives. *Frontiers in Pharmacology, 15*, 1405497. https://doi.org/10.3389/fphar.2024.1405497.

[76] Hajib, A., El Harkaoui, S., Choukri, H., Khouchlaa, A., Aourabi, S., El Menyiy, N., Bouyahya, A., & Matthaeus, B. (2023). Apiaceae family: An important source of petroselinic fatty acid—Abundance, biosynthesis, chemistry, and biological properties. *Biomolecules, 13*(11), 1675. https://doi.org/10.3390/biom13111675.
[77] Marion-Letellier, R., Savoye, G., & Ghosh, S. (2016). Fatty acids, eicosanoids, and PPAR gamma. *European Journal of Pharmacology, 785*, 44–49. https://doi.org/10.1016/j.ejphar.2016.05.015.
[78] Peng, Z., Ban, K., Wawrose, R. A., Gover, A. G., & Kozar, R. A. (2015). Protection by enteral glutamine is mediated by intestinal epithelial cell peroxisome proliferator–activated receptor-γ during intestinal ischemia/reperfusion. *Shock, 43*(4), 327–333. https://doi.org/10.1097/SHK.0000000000000294.
[79] Hsiao, Y., Su, B.-H., & Tseng, Y. J. (2020). Current development of integrated web servers for preclinical safety and pharmacokinetics assessments in drug development. *Briefings in Bioinformatics, 22*(3), bbaa124. https://doi.org/10.1093/bib/bbaa124.
[80] Michels, D., Sarah, H. E., Verkempinck, L., Van den Broeck, L., Spaepen, R., Vermeulen, K., Roelants, S., Wealleans, A., & Grauwet, T. (2025). Molecular characteristics of glycolipids determine oil–water interfacial behavior and *in vitro* lipid digestion kinetics. *Food Research International, 202*, 115714. https://doi.org/10.1016/j.foodres.2025.115714.
[81] Rivera, Z. A. A., Talubo, N. D. D., & Cabrera, H. S. (2024). Network pharmacology and molecular docking analysis of *Morinda citrifolia* fruit metabolites suggest anxiety modulation through glutamatergic pathways. *Life, 14*(9), 1182. https://doi.org/10.3390/life14091182.
[82] Hsiao, Y., Su, B.-H., & Tseng, Y. J. (2020). Current development of integrated web servers for preclinical safety and pharmacokinetics assessments in drug development. *Briefings in Bioinformatics, 22*(3), bbaa124.
[83] Hevey, R. (2019). Strategies for the development of glycomimetic drug candidates. *Pharmaceuticals, 12*. https://doi.org/10.3390/ph12020055.
[84] Li, L., Li, J., Ren, J., & Yao, J. (2025). Isorhamnetin exhibits hypoglycemic activity and targets PI3K/AKT and COX-2 pathways in type 1 diabetes. *Nutrients, 17*, Article 102. https://doi.org/10.3390/nu17203201.
[85] Kondo, H., Fujimoto, K. J., Tanaka, S., Deki, H., & Nakamura, T. (2015). Theoretical prediction and experimental verification on enantioselectivity of haloacid dehalogenase L-DEX YL with chloropropionate. *Chemical Physics Letters, 639*, 39–44.
[86] Rani, K., Kumari, P., Kumari, A., Mondal, D., Bisht, P., Kohal, R., Asati, V., Gupta, G., & Verma, S. (2025). Unveiling the medicinal diversity of benzoic acid–containing molecules: Insights on druggable targets for type 2 diabetes mellitus. *Bioorganic & Medicinal Chemistry, 128*, 118245.
[87] Liu, Y., Xie, J., Shi, Q., Gong, Q., & Qin, C. (2025). The effects of dietary supplementation with 25-hydroxyvitamin $D_3$ on the antioxidant capacity and inflammatory responses of *Pelteobagrus fulvidraco*. *Biology, 14*, Article 112.
[88] Kashyap, D., Sharma, A., Tuli, H. S., Punia, S., & Sharma, A. (2016). Ursolic acid and oleanolic acid: Pentacyclic terpenoids with promising anti-inflammatory activities. *Recent Patents on Inflammation & Allergy Drug Discovery, 10*(1), 21–33.
[89] Liu, C., Yuan, Y., Zhou, J., Hu, R., Ji, L., & Jiang, G. (2020). Piperine ameliorates insulin resistance via inhibiting metabolic inflammation in monosodium glutamate-treated obese mice. *BMC Endocrine Disorders, 20*, 44.
[90] Nurjanah, S., Gerding, A., Vieira-Lara, M., Evers, B., Langelaar-Makkinje, M., Spiekerkoetter, U., Bakker, B., & Tucci, S. (2023). Heptanoate improves compensatory mechanism of glucose homeostasis in mitochondrial long-chain fatty acid oxidation defect. *Nutrients, 15*, 3649.
[91] Ramírez, D., & Caballero, J. (2018). Is it reliable to take the molecular docking top-scoring position as the best solution without considering available structural data? *Molecules, 23*, 1038.
[92] Tsujimura, M., Ishikita, H., & Saito, K. (2025). Determinants of hydrogen bond distances in proteins. *Physical Chemistry Chemical Physics*, Advance online publication.
[93] Qi, H., & Kulik, H. J. (2019). Evaluating unexpectedly short noncovalent distances in X-ray crystal structures of proteins with electronic structure analysis. *Journal of Chemical Information and Modeling, 59*(5), 2199–2211. https://doi.org/10.1021/acs.jcim.9b00144.
[94] Vaidyanathan, R., Sreedevi, S., Ravichandran, K., Vinod, S., Krishnan, Y., Babu, L., Parthiban, P., Basker, L., Perumal, T., Rajaraman, V., Arumugam, G., Rajendran, K., & Mahalingam, V. (2023). Molecular docking approach on the binding stability of derivatives of phenolic acids (DPAs) with human serum albumin (HSA): Hydrogen bonding versus hydrophobic interactions or combined influences? *JCIS Open, 11*, 100074.